Article

Dynamics Event-Triggered-Based Time-Varying Bearing Formation Control for UAVs

Can Ding, Zhe Zhang * and Jing Zhang

College of Electrical and Information Engineering, Hunan University, Changsha 211105, China;
dingcanhn@hnu.edu.cn (C.D.); zhangj@hnu.edu.cn (J.Z.)
* Correspondence: qyzz@hnu.edu.cn

Abstract: This article addresses the leader-follower formation maneuver control problem of multiple unmanned aerial vehicles (UAVs), taking into account the time-varying velocity and time-varying relative bearing. An event-triggered bearing-based distributed velocity observer was designed, using only the desired position and velocity of the leaders. Furthermore, a dynamic event-triggered mechanism was introduced to reduce continuous communication between UAVs, thus effectively saving communication bandwidth and resources. Building on this, a bearing-only formation maneuver control strategy was proposed, integrating the event-triggered velocity observer with the backstepping control approach. To conclude, numerical simulations have been conducted to confirm the effectiveness of the proposed scheme in accomplishing formation maneuver control objectives, including translation, scaling, and rotation control. Furthermore, the advantages of the dynamic event-triggering strategy have been demonstrated through comparative simulations with traditional event-triggering strategies. Additionally, the effectiveness of the proposed observer and controller has been demonstrated by a comprehensive hardware-in-the-loop (HITL) simulation example.

Keywords: bearing-only; UAVs; dynamic event-triggered mechanism; distributed velocity observer; formation maneuver control; HITL

1. Introduction

In recent years, managing multiple unmanned aerial vehicles (UAVs) collaboratively has become a key focus in academia [1,2]. Teams of smaller, cost-effective UAVs operating in sync can perform tasks more efficiently than a single, expensive UAV. This approach highlights the significance of advanced swarm control and collision avoidance techniques. UAV swarms are now prevalent in fields like agriculture [3], search and rescue [4], environmental monitoring [5], and defense. In UAV swarm coordination, formation control is crucial, dealing mainly with two challenges: controlling formation shape and maneuvering. Formation shape control [6] involves aligning UAVs to specific geometric patterns and paths, incorporating collision avoidance [7]. Formation maneuver [8], on the other hand, focuses on the swarm's ability to move cohesively, adapt to external factors, and navigate obstacles, emphasizing real-time collision avoidance [9].

Formation control methods for the UAVs, as currently practiced, can be classified into the following three primary categories based on the type of information they measure: methods based on relative position [10–12], those founded on relative distance [13–15], and techniques derived from relative bearing [16]. The cornerstone of the method rooted in relative position is the application of the consensus algorithm [17]. This approach enables agents to achieve the targeted relative displacement by disseminating relative position data amongst neighboring UAVs. A salient benefit is its lower demand on sensor performance, striking a harmony between sensory prowess and interaction topology. Additionally, extrapolating a global control strategy from the consensus algorithm is straightforward, facilitating the easy attainment of the desired formation. In contrast, the essential tenet of the control approach based on relative distance involves agents utilizing relative distance

information between adjacent UAVs. Typically, this method necessitates that each UAV possess its own distinct local coordinate system and the competence to discern the relative positional data of neighboring UAVs. However, rigid formation control techniques might inadvertently steer the system to unintended equilibrium points, spawning undesired formation configurations. The crux of this approach then is to craft a rigid formation control strategy boasting global stability [18]. Lastly, the bearing-based control method centers around using relative bearing information. The primary objective of this strategy is to forge the desired formation structure by gauging and modulating the relative bearing in relation to neighboring UAVs. Bearing-based formation control offers distinct advantages over traditional methods rooted in relative position and distance. To begin with, it necessitates fewer sensors, which curtails both system complexity and costs. The attractiveness of bearing-based control has surged, evidenced by its integration with economical airborne optical cameras [19,20] or wireless sensor arrays [21] to capture relative bearing data. Furthermore, bearing-based strategies present a more streamlined manner to execute translation and scaling formation maneuvers control compared to their position- and distance-based strategies. This efficacy stems from the ability to maneuver formations while maintaining consistent bearing constraints, predominantly by steering the leader's motion.

Research into formation control that relies on bearing information confronts the intricacies of diverse system types. This spectrum covers first-order systems [22], progresses to second-order [23], and extends further to more advanced higher-order systems. In addition, it encompasses both linear and nonlinear systems [24], ranging from continuous to discrete system classifications. Much like traditional control fields, the research trajectory generally progresses from simpler to more complex systems, indicating a phased evolution from lower-order to higher-order systems. Trinh [25] et al., investigated the formation control problem of a single integrator in two dimensions. Notably, the controller they designed made use of only the relative bearing. Tang [26] et al., tackled the formation control challenge for time-varying relative bearing in a dimensional Euclidean space, notably by exploring the Persistence of Excitation (PE) of the desired relative direction reference point. Turning to high-order complex nonlinear intelligence, Zhao [27] et al., developed a bearing-only distributed formation controller for a high-order complex multi-intelligence system, specifically those with moving targets. Lastly, Wu [28] et al., delved into finite-time formation tracking control for heterogeneous mobile robots. In the above-mentioned bearing information-based formation control, the expected formation structure is constrained by the relative bearing information. Interestingly, while this bearing information depends on the global coordinates, there is a notable shift to avoid such global information in distributed formation controllers. Consequently, scholars have proposed local coordinate-based formation controllers that incorporate bearing information. Garanayak [29] et al., designed bearing-based formation controllers under local references. Their aim was to accomplish the task of fixed-point formation with bounded perturbations for both single-integrator and double-integrator systems. Luo [30] et al., put forth a distributed global stabilization controller based on inverse information. Significantly, by minimizing the cost function under the optimal rotation matrix, their proposal solely relies on local orientation measurements. On a different note, Zhang [31] et al., designed a distributed orientation estimation method. This method determines the orientation of the follower under the first leader coordinate system, thereby sidestepping any dependence on global position or coordinates. Building on this, they then combined the orientation information with the formation controller to successfully accomplish the UAV formation task.

Nevertheless, a majority of the aforementioned studies operate under the assumption that both the desired velocity and the relative bearing remain constant over time. However, when the formation system is tasked with complex operations such as translation, rotation, and scaling, adjustments in velocity and relative bearing become imperative. This is compounded by the fact that bearing information mainly reflects the inverse tangent relationships between agents' displacements. Relying on such bearings for control strategies is fraught with challenges, especially when these desired bearings are variable over time [32].

Additionally, the studies previously mentioned operate under the presumption that proximate UAVs maintain continuous communication. However, sustaining such continuous communication is evidently impractical on a digital control platform [33]. Taking into account the limitations of sampling frequency and communication bandwidth updates in real-world formation control systems, there emerges an urgent need to formulate strategies that bypass this continuous paradigm and reduce superfluous communications.

Inspired by the aforementioned discourse, we delve into the matter of event-triggered, bearing-only formation maneuver control for UAVs. To address the challenges posed by unknown time-varying velocities and relative bearings, we proposed an event-triggered distributed velocity observer. By integrating backstepping control methods, we effectively addressed the formation maneuver control challenge. The primary contributions of this paper can be summarized as follows:

First, a dynamic event-triggered distributed velocity observer was proposed to handle the time-varying relative bearing. Compared with [27–31], which were developed for the constant velocity formation tracking mission, the proposed method can address the time-varying formation problems. Second, a dynamic event-triggered mechanism is developed to avoid continuous communication between UAVs and thus save resources. Lastly, a bearing-only backstepping formation control strategy, combined with the event-triggered velocity observer, was proposed, and the formation maneuver problem was solved.

The structure of the remaining sections in this paper is as follows: Section 2 provides an introduction to the preliminary concepts, and presents the problem formulation. Section 3 introduced the event-triggered-based distributed velocity observer. In Section 4, bearing-only formation control is proposed. The simulation results are shown in Section 5.

2. Preliminaries and Problem Formulation

Notations: In this section, the set of real numbers and non-negative real numbers is denoted by R and R^+, respectively, $R^{n \times m}$ and R^n are the set of $n \times m$ real matrices and $n \times 1$ real vectors, respectively. $\|A\|$ is the 2-norm of the matrix A. I_d is the $d \times d$ identity matrix. $col(x_1, x_2, \cdots, x_n)$ is column stack with x_i over i from 1 to n, $col(x_1, x_2, \cdots, x_n) = [x_1^T, x_2^T, \cdots, x_n^T]^T$. $\lambda_{\max}(\cdot)$ and $\lambda_{\min}(\cdot)$ represent the maximum eigenvalue and minimal eigenvalue of matrix, respectively. $\lambda_m(\cdot)$ denotes the largest absolute value of the eigenvalues of a matrix.

2.1. System Model of UAVs

Consider a group of n UAV moving in $R^d, d = 3$. Suppose the first $n_l \geq 2$, UAV are leaders and the rest, $n_f = n - n_l$ UAV, are followers. Denote the position and velocity of *ith* UAV are $p_i \in R^d$ and $v_i \in R^d$, respectively. Specifically, the leaders are assumed to move in the desired position and desired velocity without control, which means $p_i = p_i^*$, $v_i = v_i^*, i \in n_l$, where p_i^* and v_i^* denote the desired position and velocity, respectively.

In exploring the formation control of UAVs, it is evident that the response time for trajectory adjustments of UAVs is significantly longer than that for attitude adjustments. Therefore, in formation control strategies involving only position and velocity, a hierarchical control approach can be adopted, with an inner loop and an outer loop structure. This paper's primary focus lies on the outer-loop control, allowing the UAV's dynamic model to be approximated by a double integrator [34]. Building on this approximation, the dynamic of a group of *ith* UAVs can be described as follows:

$$\dot{p}_i = v_i, \dot{v}_i = u_i, i \in n_f \tag{1}$$

where u_i expressed the control input of *ith* UAV.

Remark 1. *From the perspective of formation control, simplifying each UAV to a point mass model is done for the sake of simplicity in control algorithm design and validation. Using a point mass model effectively reduces the complexity of the model, making the formation control strategy*

easier to implement and analyze. Although this simplification neglects some real-world dynamic characteristics such as air resistance and non-linear dynamics, it still effectively captures the core of the problem—adjustments in position and velocity—and can describe the basic behavior of UAVs in formation flight for the majority of scenarios.

Assumption 1 (Interagent collision avoidance). *Collision avoidance between each couple of UAVs is guaranteed during the formation tracking evolvement, i.e., $p_i \neq p_i$ for all $i \neq j$ and $t \geq 0$.*

Remark 2. *This critical assumption maintains the integrity of the mission and reduces risks associated with potential overlaps or close encounters. Indeed, this assumption is not just a practical necessity; it is also a vital research area within the discipline of formation control. For those intrigued by this subject, a comprehensive exploration can be found in the existing literature [24–31].*

2.2. Basic Graph Theory

Denote the topology of n UAV formation systems as a graph $G = (V, \varepsilon)$ consisting of a node set $V = \{1, 2, \cdots, n\}$ and an edge set of $\varepsilon = \{(i, j) : i \neq j, i, j \in V\}$. The edge number of edge set ε is m and the edge $(i, j) \in \varepsilon$ means that the ith UAV can measure the relative bearing information and receive the information from jth UAV by communication technologies. Denote the set of neighbors of UAV i as $N_i := \{j \in V : (i, j) \in \varepsilon\}$. Let $V = V_l \cup V_f$, where $V_l = \{1, \cdots, n_l\}$, $V_f = \{n_{l+1}, \cdots, n\}$ denote the sets of leaders and followers, respectively. The edges crossing the set V_l and V_f are directed, which means only the followers can measure and receive the information from the leaders. The edges among V_f are undirected. For any edge $(i, j) \in \varepsilon$, we define the relative displacement vector and relative bearing vector as $e_{ij} = p_j - p_i$ and $g_{ij} = e_{ij}/\|e_{ij}\|$, respectively. For ease in notation, we will use e_k and g_k instead of e_{ij} and g_{ij}, respectively, where k ranges over $\{1, 2, \cdots, m\}$.

The bearing Laplacian matrix B for graph G is defined as follows:

$$[B_{ij}] = \begin{cases} 0_{d \times d}, i \neq j, (i, j) \notin \varepsilon \\ -P_{g_{ij}}, i \neq j, (i, j) \in \varepsilon \\ \sum_{k \in N_i} P_{g_{ik}}, i = j, i \in \varepsilon \end{cases}$$

where $P_{g_{ij}} \in R^{d \times d}$ orthogonal projection matrix of bearing g_{ij} and $P_{g_{ij}} = I_d - g_{ij}g_{ij}^T$.

Given the separation of the leader and follower UAVs, matrix B can be segmented into the following components:

$$B = \begin{bmatrix} B_{ll} & B_{lf} \\ B_{fl} & B_{ff} \end{bmatrix}$$

where $B_{ll} \in R^{dn_l \times dn_l}$, $B_{lf} \in R^{dn_l \times dn_f}$, $B_{fl} \in R^{dn_f \times dn_l}$ and $B_{ff} \in R^{dn_f \times dn_f}$.

Several lemmas and corollaries that will be utilized in this paper are now introduced.

Lemma 1 (Uniqueness of target formation [35]). *The target framework (G, p^*) is unique, where $p^* = col(p_1^*, p_2^*, \cdots, p_n^*)$ is the desired position, if and only if B_{ff} is positive definite. This means that the desired position $p_i^*, i \in n_f$ and velocity $v_i^*, i \in n_f$ of the followers can be uniquely determined by the leaders' position $p_i^*, i \in n_l$ and velocity $v_i^*, i \in n_l$. Moreover, the desire position and velocity of the follower can be deduced by the following equation:*

$$\begin{cases} p_f^* = -B_{ff}^{-1} B_{fl} p_l^* \\ v_f^* = B_{ff}^{-1}((\dot{B}_{ff} B_{ff}^{-1} B_{fl} - \dot{B}_{fl}) p_l^* - B_{fl} v_l^*) \end{cases} \quad (2)$$

where $p_l^* = col(p_1^*, \cdots, p_{n_l}^*)$, $v_l^* = col(v_1^*, \cdots, v_{n_l}^*)$, $p_f^* = col(p_{n_l+1}^*, \cdots, p_n^*)$, $v_f^* = col(v_{n_l+1}^*, \cdots, v_n^*)$.

Assumption 2. *The desired position p_l^*, desired velocity v_l^*, its first-order derivative $\dot{v}_l^*$, the desired relative bearing g^* and its first-order derivative $\dot{g}^*$ are all bounded.*

Lemma 2 (Schur complement). *Consider the block matrix below, partitioned in the following way:*

$$M = \begin{bmatrix} A & B \\ B^T & C \end{bmatrix}$$

Then, the block matrix M is definite if and only if A is definite and the Schur complement $C - B^T A^{-1} B$ of the matrix M is definite, or C is definite and the Schur complement $A - B C^{-1} B^T$ of the matrix M is definite.

Lemma 3 (Work of [36]). *Consider a matrix $M > 0$ shown in Lemma 2 and define vector $x \in R^{d_A}$ and $y \in R^{d_C}$, where d_A and d_C represent the dimension of the matrix A and C, respectively. Then there holds the following:*

$$\lambda_{\min}(M_1) x^T x \leq x^T M_1 x \leq col^T(x, y) M col^T(x, y)$$
$$\lambda_{\min}(M_2) y^T y \leq y^T M_2 y \leq col^T(x, y) M col^T(x, y)$$

where $M_1 = A - B C^{-1} B^T$, $M_2 = C - B^T A^{-1} B$.

2.3. Problem Formulation

In this paper, the control objective is to design the bearing-based control input u_i for the follower UAV to accomplish the formation maneuver mission. Define $g = col(g_1, g_2, \cdots, g_m), g^* = col(g_1^*, g_2^*, \cdots, g_m^*), v_f = col(v_{n_l+1}, \cdots, v_n)$.

Definition 1 (Target formation). *A formation (p_f, g, v_f) is defined as a target formation if $p_f = p_f^*, v_f = v_f^*, g = g^*$.*

Remark 3. *The static formation with $v_f^* = 0$ and the tracking formation with constant velocity, $\dot{v}_f^* = 0$, have been extensively studied in various literature sources. In contrast, the time-varying velocity, particularly the time-varying bearing, in the bearing-based formation approach has seldom been explored. In this paper, we focus on the time-varying velocity and bearing scenario, and investigate the translation, scaling, and rotation maneuvers within the formation mission by altering the velocity, desired position, and desired bearing.*

The desired position and velocity of each follower can be determined with certainty only if the bearing-based formation is unique. To ensure the uniqueness of the target formation, we invoke Lemma 1 and make the following assumption:

**Assumption 3.** *The graph G is connected, and the matrix B_{ff} satisfies the definite condition.*

Assumption 4. *The leader of the UAV formation systems follows the desired tracking trajectory without control, i.e., $p_i = p_i^*, v_i = v_i^*, i \in V_l$.*

Remark 4. *Assumptions 3 and 4 are prevalent in the bearing-based formation control problem with a leader-follower structure [37–39]. Given that the formation controls designed are unavailable for the unique target formation, Assumption 3 is fundamental for the leader-follower structured UAV problem, as stipulated by Lemma 1. We recognize that leaders usually follow set reference paths rather than dynamic controls. Such deviations can impact the whole formation significantly. Our study specifically targets follower controllers to refine strategies within this framework, ensuring our main goals are achieved without dilution. Future research could explore the effects of leader behavior changes to improve system robustness.*

Problem 1. *Consider a group of n UAVs, composed of n_l leaders and n_f followers, where the leaders can transmit the desired position p_l^* and desired velocity v_l^* to the followers. Utilizing the relative bearing information, along with the desired position and velocity of the leader, we design distributed velocity observers and controllers for the followers. This design ensures that the*

target formation described in Definition 1 can be achieved and accomplish the formation maneuver control mission.

Figure 1 displays the schematic diagram of the formation maneuver control. It stands in contrast to the traditional formation tracking control where the relative bearing, velocity, and distance between leaders remain time-invariant. In maneuver control, changes in relative bearing and desired velocity are introduced, rendering them time-varying. This adaptation enables the achievement of translation, scaling, and rotation maneuver control targets.
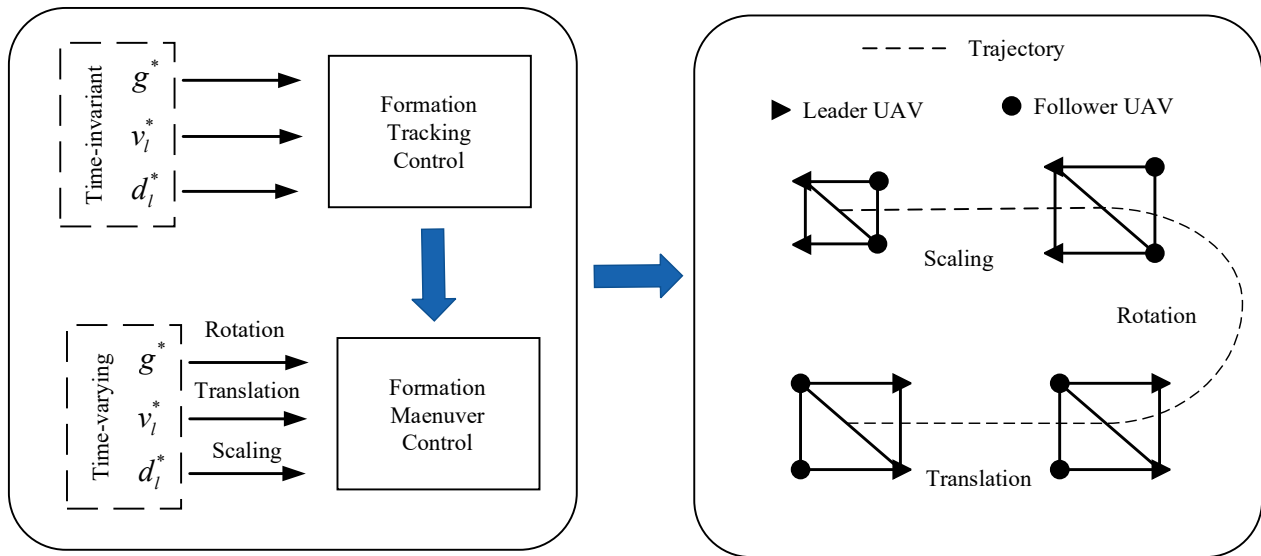
Figure 1. Schematic diagram of formation maneuver control.

3. Dynamic Event-Triggered Based Distributed Velocity Observer

According to Lemma 1, the followers' desired velocity is influenced by the leaders' desired position and velocity, and the matrices B_{ff}, B_{lf}, and $\dot{B}_{ff}$, which encapsulate the knowledge of the communication network topology. Consequently, it becomes necessary to formulate a distributed estimator. This estimator, reliant on local information regarding the neighbors, enables each follower to gauge its desired states accurately. In addition, the limited network bandwidth of formation systems precludes the use of traditional continuous transmission methods. As a consequence, it becomes essential to innovate an event-triggered communication strategy. This approach ensures that communication is carried out only when absolutely necessary, effectively eliminating the need for continuous transmission.

Firstly, define the following error function:

$$m_i(t) = -a_1 \left(\sum_{j \in N_i} B_{ij} (\hat{v}_i - \hat{v}_j) + \sum_{j \in N_i} M_{ij} (\hat{p}_i - \hat{p}_j) \right), i \in V_f \tag{3}$$

where $M_{ij} = \dot{B}_{ij} + a_2 B_{ij}$, a_1 and a_2 are positive constant gain, $\hat{v}_i$ and $\hat{p}_i$ denote the estimation of the desired velocity v_i^* and desired position p_i^*, respectively, for the follower *ith* UAV. $\hat{v}_j$ and $\hat{p}_j$ represent the estimation information received from the neighbor *jth* UAV. If the neighboring UAV is one of the leaders, which means that the *ith* UAV can receive the information from the leader j, then $\hat{v}_j = v_j^*$, $\hat{p}_j = p_j^*$, $j \in V_l$.

Assume the event-triggered time sequence of the follower UAV i is $t_0^i, t_1^i, \cdots, t_k^i, \cdots$, and define the event-triggered state as follows:

$$\begin{cases} \overline{v}_i(t) = \hat{v}_i(t_k^i), \overline{p}_i = \hat{p}_i(t_k^i), i \in V_f \\ \overline{v}_i(t) = v_i^*(t_k^i), \overline{p}_i = p_i^*(t_k^i), i \in V_l \end{cases}, \forall t \in \left[t_k^i, t_{k+1}^i\right) \tag{4}$$

The event-triggered error function for the follower UAV i as follows:

$$\overline{m}_i(t) = -a_1 \left(\sum_{j \in N_i} B_{ij} \left(\overline{v}_i(t_k^i) - \overline{v}_j(t_k^i) \right) + \sum_{j \in N_i} M_{ij} \left(\overline{p}_i(t_k^i) - \overline{p}_j(t_k^i) \right) \right), i \in V_f \tag{5}$$

Further, we define the velocity mismatch and position mismatch for UAV i between consecutive event times $t \in \left[t_k^i, t_{k+1}^i\right)$ as follows:

$$\begin{cases} e_i(t) = \overline{v}_i(t_k^i) - \hat{v}_i(t) \\ z_i(t) = \overline{p}_i(t_k^i) - \hat{p}_i(t) \end{cases}, \forall t \in \left[t_k^i, t_{k+1}^i\right) \tag{6}$$

With these definitions, the event-triggered error function (5) can be reformulated.

$$\overline{m}_i(t) = m_i(t) - a_1 \left(\sum_{j \in N_i} B_{ij}(e_i(t) - e_j(t)) \right) - a_1 \left(\sum_{j \in N_i} M_{ij}(z_i(t) - z_j(t)) \right) \tag{7}$$

Let $M_{ff} = \dot{B}_{ff} + a_2 B_{ff}$, $M_{fl} = \dot{B}_{fl} + a_2 B_{fl}$. In a more compact representation, the above equation becomes the following:

$$\overline{m}(t) = -a_1 \left(B_{ff} \hat{v}_f + M_{ff} \hat{p}_f \right) - a_1 \left(B_{fl} v_l^* + M_{fl} p_l^* \right) - a_1 \left(B_{ff} e_f + \dot{B}_{ff} z_f \right) - a_1 \left(B_{fl} e_l + \dot{B}_{fl} z_l \right) \tag{8}$$

where $\hat{v}_f = col(\hat{v}_{n_l+1}, \cdots, \hat{v}_n)$, $\hat{p}_f = col(\hat{p}_{n_l+1}, \cdots, \hat{p}_n)$, $e_f = col(e_{n_l+1}, \cdots, e_n)$, $z_f = col(z_{n_l+1}, \cdots, z_n)$, $e_l = col(e_1, \cdots, e_{n_l})$, $z_l = col(z_1, \cdots, z_{n_l})$, $\overline{m} = col(\overline{m}_{n_l+1}, \cdots, \overline{m}_n)$.
According to the Lemma 1, we have the following:

$$B_{ff} p_f^* + B_{fl} p_l^* = 0 \tag{9}$$

$$\dot{B}_{ff} p_f^* + B_{ff} v_f^* + \dot{B}_{fl} p_l^* + B_{fl} v_l^* = 0 \tag{10}$$

Let $\tilde{v}_f = \hat{v}_f - v_f^*$, $\tilde{p}_f = \hat{p}_f - p_f^*$. Combined with the Equations (3), (9) and (10), we have the following:

$$\begin{aligned} \overline{m}(t) &= -a_1 \left(B_{ff} \tilde{v}_f + M_{ff} \tilde{p}_f \right) - a_1 \left(B_{ff} v_f^* + M_{ff} p_f^* + B_{fl} v_l^* + M_{fl} p_l^* \right) \\ &\quad -a_1 \left(B_{ff} e_f + M_{ff} z_l \right) - a_1 \left(B_{fl} e_l + M_{fl} z_l \right) \\ &= -a_1 \left(B_{ff} \tilde{v}_f + M_{ff} \tilde{p}_f \right) - a_1 \left(B_{ff} e_f + M_{ff} z_l \right) - a_1 \left(B_{fl} e_l + M_{fl} z_l \right) \end{aligned} \tag{11}$$

It should be noted that the design of the distributed velocity observer, which includes the term $M_{ij} = \dot{B}_{ij} + a_2 B_{ij}$, is founded on Lemma 1 and Equations (9) and (10). This formulation transforms the error equation into a function comprising both the velocity estimation error $\tilde{v}_f$ and the position estimation error $\tilde{p}_f$. Such configuration is crucial for maintaining the stability of the closed-loop control system. Additionally, the velocity observer operates using only the local information from neighboring UAVs, thereby eliminating the need for global information from the formation system.

Then, the triggering function can be formulated as follows:

$$d_i(t) = \delta_i(t) - c_1 \|\overline{m}_i(t)\|^2 \tag{12}$$

where $\delta_i(t) = \sum\limits_{j \in V_f} \left(\|B_{ij}e_i\|^2 + \|M_{ij}z_i\|^2 \right) + \frac{1}{2} \sum\limits_{j \in V_l} \left(\|B_{ij}e_j\|^2 + \|M_{ij}z_j\|^2 \right)$, c_1 is positive constant.

Define the following dynamic variable for the follower UAV:

$$\dot{\alpha}_i(t) = c_2 \alpha_i(t) - c_3 d_i(t), i \in V_f, t \in [t_k^i, t_{k+1}^i) \tag{13}$$

where c_2 and c_3 are the positive constant, and the initial value of the dynamic variable $\alpha_i(t)$ is greater than zero, $\alpha_i(0) > 0$.

Then, the event-triggered mechanism can then be designed as follows:

$$t_{k+1}^i = \inf\left\{ t > t_k^i, \alpha_i(t) - c_4 \|d_i(t)\| > 0 \right\}, i \in V_f \tag{14}$$

It is worth noting that the dynamic variable $\alpha_i(t)$ plays a crucial role in dynamically adjusting the threshold. When $\alpha_i(t)$ is set to zero, the mechanism shifts to the traditional static event-triggered method. The introduction of the variable $\alpha_i(t)$ can produce larger triggering intervals and reduce triggering times, which will be demonstrated in the subsequent comparison simulations.

Further, the event-triggered-based distributed velocity observer can be designed as follows:

$$\begin{cases} \dot{\tilde{p}}_f = \tilde{v}_f \\ \dot{\tilde{v}}_f = \overline{m} \end{cases} \tag{15}$$

The main result for this section is presented as follows:

Theorem 1. *Given that Assumption 2 is valid and the constant parameter adheres to the subsequent condition:*

$$a_1 > \max\left\{ \lambda_m\left(B_{ff}^{-1}\left(M_{ff} + \frac{1}{2}\dot{B}_{ff} \right) B_{ff}^{-1} \right), \frac{4a_2}{a_3} \lambda_m\left(M_P B_{ff}^{-1} M_P \right) \right\} \tag{16a}$$

$$a_2 > \max\left\{ \lambda_m\left(B_{ff}^{-1/2}\dot{B}_{ff}B_{ff}^{-1/2} \right), \lambda_m\left(B_{ff}^{-1}\dot{B}_{ff}^2 B_{ff}^{-1} \right) \right\} \tag{16b}$$

$$a_3 > \lambda_m\left(a_2^2 M_{ff} B_{ff}^{-1} M_{ff} \right) \tag{16c}$$

$$\theta_1 > 0, \theta_2 > 0 \tag{16d}$$

where

$$M_P = \frac{1}{2}(\dot{M}_{ff} + a_3 I_{dn_f}). \; M_1 = A - BC^{-1}B^T, \; M_2 = C - B^T A^{-1}B,$$
$$\theta_1 = \lambda_{\min}(M_1) - \lambda_{\max}^2\left(M_{ff} \right) - 4a_1^2 c_1 c_3 \lambda_1 n_f,$$
$$\theta_2 = \lambda_{\min}(M_2) - \lambda_{\max}^2\left(B_{ff} \right) - 4a_1^2 c_1 c_3 \lambda_2 n_f, \; A = a_1 M_{ff}^2,$$
$$B = a_1 M_{ff} B_{ff} - \frac{1}{2}(\dot{M}_{ff} + a_3 I_{dn_f}), \; C = a_1 B_{ff}^2 - M_{ff} - \frac{1}{2}\dot{B}_{ff}.$$

Then, utilizing the distributed velocity (15) with the event-triggered mechanism (14) for the follower UAV and the parameters event-trigger parameter satisfies.

$$c_3 = 3a_1^2/(1 - 2a_1^2 c_1) > 0 \tag{17}$$

Then, the estimation errors $\tilde{p}$ and $\tilde{v}$ converge globally asymptotically, where $\tilde{p} = \hat{p} - p^*$, $\tilde{v} = \hat{v} - v^*$. Meanwhile, the minimal interevent interval is positive, and the Zeno phenomenon is eliminated.

Proof. See Appendix A.1.

4. Bearing-Only Formation Control Design

In this section, a bearing-only distributed formation controller was designed to follow UAVs so that Problem 1 can be achieved. Combined with the distributed velocity observer, the maneuver formation mission with time-varying velocity and time-varying relative bearing was accomplished.

Firstly, define the velocity tracking error of the UAV formation system as $v_i^e = v_i - \hat{v}_i, i \in V_f, v_i^e = 0, i \in V_l$, and $v^e = col(v_1^e, v_2^e, \cdots, v_n^e)$.

Consider the following Lyapunov candidate function:

$$V_2 = \frac{1}{2} \sum_{i=n_f} \sum_{(i,j)\in\varepsilon} \left(g_{ij} - g_{ij}^*\right)^T \left(g_{ij} - g_{ij}^*\right) \tag{18}$$

Then, the derivate of the function V_2 is as follows:

$$
\begin{aligned}
\dot{V}_2 &= \sum_{i=1}^{n} \sum_{j\in N_i} \tilde{g}_{ij}^T P_{g_{ij}}(v_i - v_j)/\|e_{ij}\| + \sum_{i=1}^{n} \sum_{j\in N_i} \tilde{g}_{ij}^T \dot{g}_{ij}^* \\
&= \sum_{i=1}^{n} \sum_{j\in N_i} \tilde{g}_{ij}^T P_{g_{ij}}(v_i^e - v_j^e)/\|e_{ij}\| + \sum_{i=1}^{n} \sum_{j\in N_i} \tilde{g}_{ij}^T P_{g_{ij}}(\hat{v}_i - \hat{v}_j)/\|e_{ij}\| + \sum_{i=1}^{n} \sum_{j\in N_i} \tilde{g}_{ij}^T \dot{g}_{ij}^*
\end{aligned}
\tag{19}
$$

According to the bearing rigidity matrix $R(p)$, the above equation can be rewritten as the following compact form:

$$\dot{V}_2 = \tilde{g}^T R v^e + \tilde{g}^T R \hat{v} + \tilde{g}^T \dot{g}^* \tag{20}$$

where $\tilde{g} = col(\tilde{g}_1, \tilde{g}_2, \cdots, \tilde{g}_m)$, $\dot{g}^* = col(\dot{g}_1^*, \dot{g}_2^*, \cdots, \dot{g}_m^*)$.

Then, introduce the following virtual control variable:

$$\alpha = -k_v R^T \tilde{g}^T \tag{21}$$

In addressing Problem 1, the controller design is mandated to fulfill the bearing-only based condition. Evidently, the virtual control incorporates the distance norm $\|e_{ij}\|$, rendering it unsuitable for controller design. Given this constraint, we adapt the virtual control variables in the subsequent manner:

$$\alpha = -k_v \overline{R}^T \tilde{g}^T \tag{22}$$

where $\overline{R} = diag(P_{g_k})\overline{H}$, without the distance norm $\|e_{ij}\|$, k_v is positive controller parameter.

The auxiliary variable is designed as follows:

$$s = v^e - \alpha \tag{23}$$

Then, consider the following Lyapunov function:

$$V_3 = V_2 + \frac{1}{2} s^T s \tag{24}$$

The derivative of the above Lyapunov function is given as follows:

$$\dot{V}_3 = \tilde{g}^T \overline{R} v^e + \tilde{g}^T \overline{R} \hat{v} + \tilde{g}^T \dot{g}^* + s^T (u - \dot{\hat{v}} - \dot{\alpha}) \tag{25}$$

where $u = col(u_1, u_2, \cdots, u_n)$, $u_i = 0, i \in V_l$.

Then, inspired by the reference [40], the maneuver formation control law for the UAVs is designed as follows:

$$\begin{cases} u = -k_c s - \overline{R}^T \tilde{g} + \dot{\hat{v}} + \dot{\alpha} \\ \alpha = -k_v \overline{R}^T \tilde{g}^T \end{cases} \tag{26}$$

Remark 5. *The control parameters k_c and k_v are crucial for minimizing convergence error. Increasing k_c and k_v enhances the system's response speed by reducing the time required to correct bearing and velocity errors, thus improving the control system's effectiveness in achieving target speed and bearing swiftly. Accelerated convergence of these errors leads to better control performance and a more responsive adaptation to trajectory changes. However, careful calibration of k_c and k_v is essential. Overly high values may cause the system to overshoot the desired trajectory, leading to potential instability or oscillatory behavior.*

The control block diagram of the formation maneuver system is shown in Figure 2.
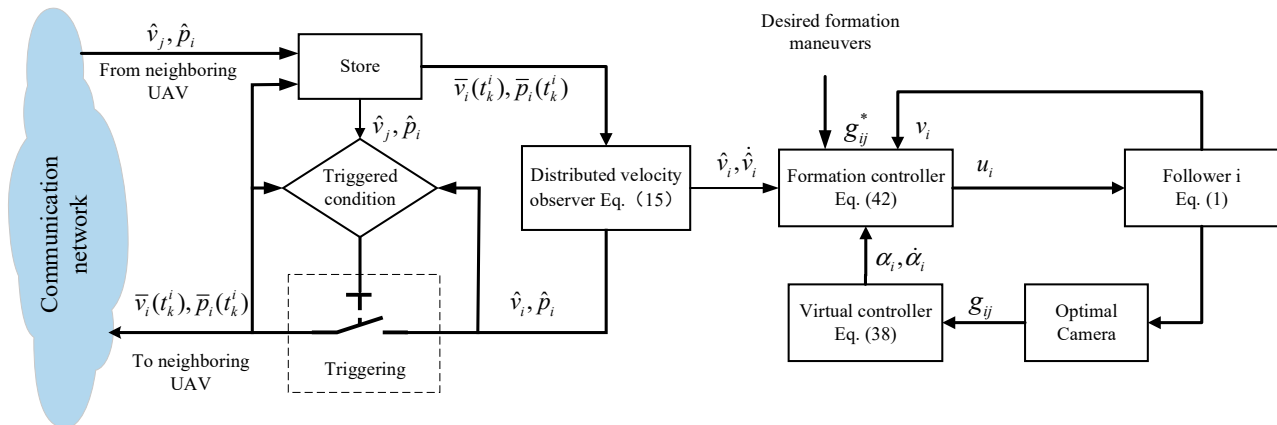
Figure 2. Control block diagram of the formation maneuver system.

Theorem 2. *Given that Assumptions 1–4 are valid, the distributed velocity estimator and the formation maneuver controller are designed as per (15) and (26), respectively, and the control parameter satisfies the following:*

$$k_v > \frac{\left(\lambda_{\max}(\overline{R}) - 1\right)}{2\lambda_{\min}(\overline{R}^T \overline{R})}$$

Problem 1 can be solved.
Proof. See Appendix A.2.

Remark 6. *Contrary to traditional velocity observer-based bearing-only formation control methods [41], an event-triggered mechanism was introduced to reduce continuous communication and conserve resources. This modification results in the velocity estimation error only being able to asymptotically converge to zero, rather than achieving exponential convergence. Therefore, the controller (26) designed in this paper merely ensures that the tracking errors are UUB.*

5. Simulation Examples

In the simulation experiments, we conducted two distinct cases to evaluate the performance of the proposed controller. The first case aimed to demonstrate the effectiveness of the translation and scaling maneuver formation control of the proposed controller. The second case is used to verify the rotation maneuver formation control of the proposed methods in this paper. Figure 3 shows the target formation structure and the communication topology structure for the simulation examples.
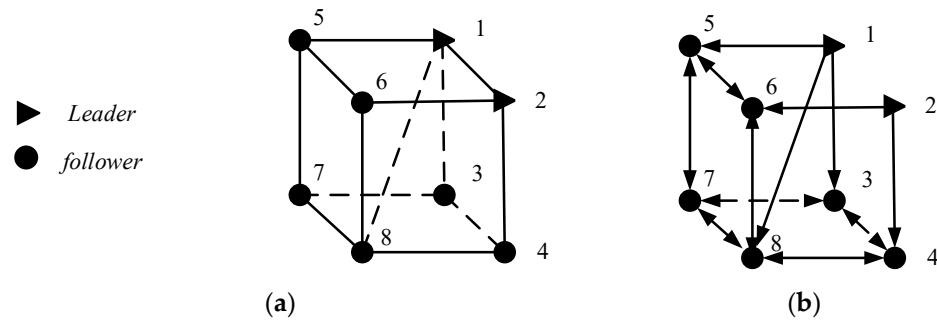
Figure 3. The target formation structure (**a**) and communication topology structure (**b**).

5.1. Translation and Scaling Formation Control for UAV

In this subsection, we evaluate the translation and scaling effects of the UAV formation system through simulation experiments. These experiments not only validate our control strategy but also provide valuable insights into the system's behavior. The desired formation structure is a cube, as depicted in Figure 3a. To ensure effective communication and coordination among the UAVs, we have designed a specific communication structure, which is illustrated in Figure 3b. During the translation and scaling formation simulations, the desired relative bearings for the formation system remain time-invariant, with values of $g_{82}^* = 1/\sqrt{3}[1 \quad 1 \quad 1]^T$, $g_{32}^* = g_{41}^* = g_{76}^* = g_{85}^* = [1 \quad 0 \quad 0]^T$, $g_{43}^* = g_{56}^* = g_{87}^* = [0 \quad 1 \quad 0]^T$, $g_{51}^* = g_{62}^* = g_{73}^* = g_{84}^* = [0 \quad 0 \quad 1]^T$, and other relative bearing information can be obtained by $g_{ij}^* = -g_{ij'}^*$, $(i, j) \in \varepsilon$. The initial positions of the leaders are $p_1(0) = [4 \quad 0 \quad 4]^T m$, $p_2(0) = [4 \quad 4 \quad 4]^T m$, respectively. The initial positions of the followers are $p_3(0) = [3 \quad 2 \quad 3]^T m$, $p_4(0) = [2 \quad -1 \quad 4]^T m$, $p_5(0) = [3 \quad -0.1 \quad 5]^T m$, $p_6(0) = [3 \quad 3 \quad -1]^T m$, $p_7(0) = [-1 \quad 5 \quad 1]^T m$, $p_8(0) = [0 \quad 3 \quad -1]^T m$, while their velocities are set to zero. The control parameters of the controller are selected as $k_v = 54$, $k_c = 2$, $a_1 = 5$, $a_2 = 0.3$, $c_1 = 1$, $c_2 = 0.07$. The velocity of the first leader is as follows:

$$\text{Translation}: \begin{cases} v_1 = \begin{bmatrix} \sin(\pi t/40) & 0 & \cos(\pi t/40) \end{bmatrix}^T, 0 \leq t < 20 \\ v_1 = \begin{bmatrix} \cos(\pi(t-50)/40) & 0 & \sin(\pi(t-50)/40) \end{bmatrix}^T, 50 \leq t \leq 70 \end{cases} \quad (27)$$

$$\text{Scaling}: \begin{cases} v_1 = \begin{bmatrix} 1 & 0.2\sin(\pi(t-10)/10) & -0.2\sin(\pi(t-10)/10) \end{bmatrix}^T, 20 \leq t < 30 \\ v_1 = \begin{bmatrix} 1 & 0 & 0 \end{bmatrix}^T, 30 \leq t < 40 \\ v_1 = \begin{bmatrix} 1 & -0.2\sin(\pi(t-40)/10) & 0.2\sin(\pi(t-40)/10) \end{bmatrix}^T, 40 \leq t < 50 \end{cases} \quad (28)$$

The velocity of the second leader is as follows:

$$\text{Translation}: \begin{cases} v_2 = \begin{bmatrix} \sin(\pi t/40) & 0 & \cos(\pi t/40) \end{bmatrix}^T, 0 \leq t < 20 \\ v_2 = \begin{bmatrix} \cos(\pi(t-50)/40) & 0 & \sin(\pi(t-50)/40) \end{bmatrix}^T, 50 \leq t \leq 70 \end{cases} \quad (29)$$

$$\text{Scaling}: \begin{cases} v_2 = \begin{bmatrix} 1 & -0.2\sin(\pi(t-10)/10) & -0.2\sin(\pi(t-10)/10) \end{bmatrix}^T, 20 \leq t < 30 \\ v_1 = \begin{bmatrix} 1 & 0 & 0 \end{bmatrix}^T, 30 \leq t < 40 \\ v_2 = \begin{bmatrix} 1 & 0.2\sin(\pi(t-40)/10) & 0.2\sin(\pi(t-40)/10) \end{bmatrix}^T, 40 \leq t < 50 \end{cases} \quad (30)$$

The UAV formation system executes the translation maneuver formation with time-varying velocity from 0 to 20 s and again from 50 to 70 s. The system accomplishes the scaling maneuver formation between 20 to 30 s and 40 to 50 s. Additionally, the translation maneuver with a constant velocity is carried out from 30 to 40 s.

The simulation results are shown in Figures 4–8.
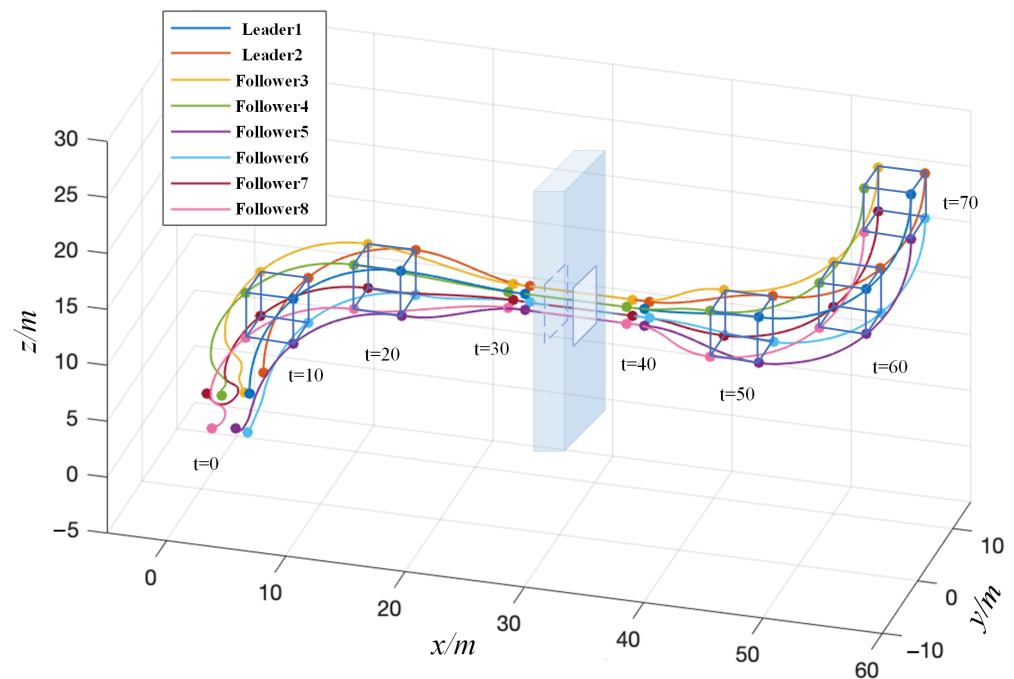
Figure 4. The translation and scaling formation control effects.
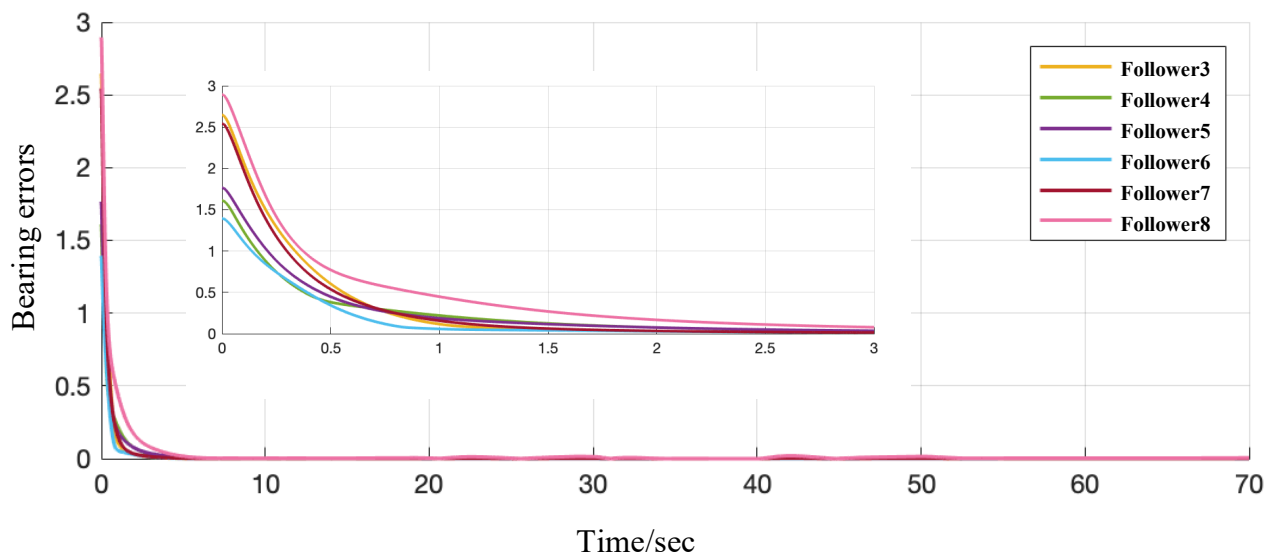
Figure 5. The bearing error $\sum\limits_{(i,j)\in\varepsilon} \|g_{ij} - g_{ij}^*\|$ of the follower UAVs.

From Figure 4, the distributed formation controller proposed in this study effectively accomplishes the prescribed translation and scaling maneuver formations. As depicted in both Figures 5 and 6, the formation system adeptly tracks the desired relative bearing and velocity. Figure 7 illustrates the proficiency of the velocity observer designed in this paper in effectively estimating the desired formation velocity information. It is pertinent to highlight that the desired formation velocity is derived from Lemma 1. Figure 8 captures the event-triggering moments for each follower UAV, signifying communication occurs solely when the triggering condition is met. Consequently, this leads to efficient utilization and the saving of control system resources.
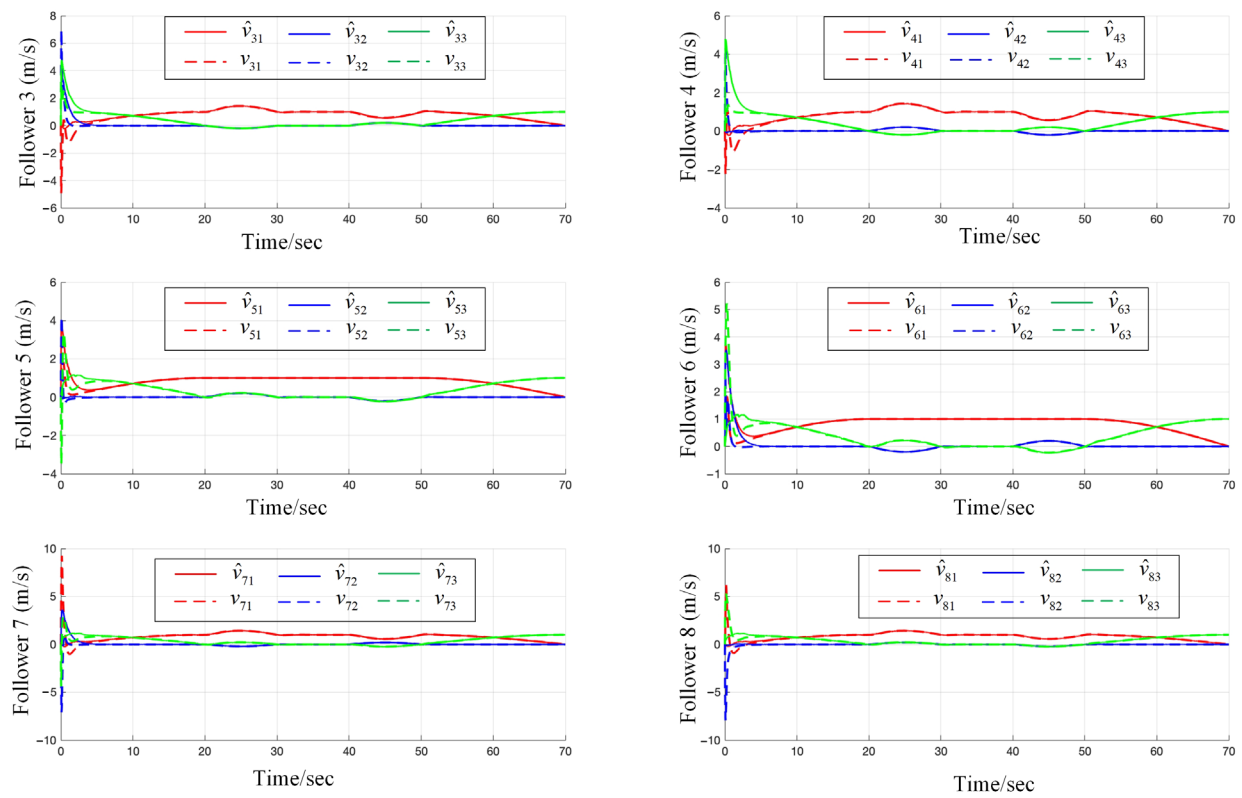
Figure 6. The velocity tracking effect of the follower UAVs.
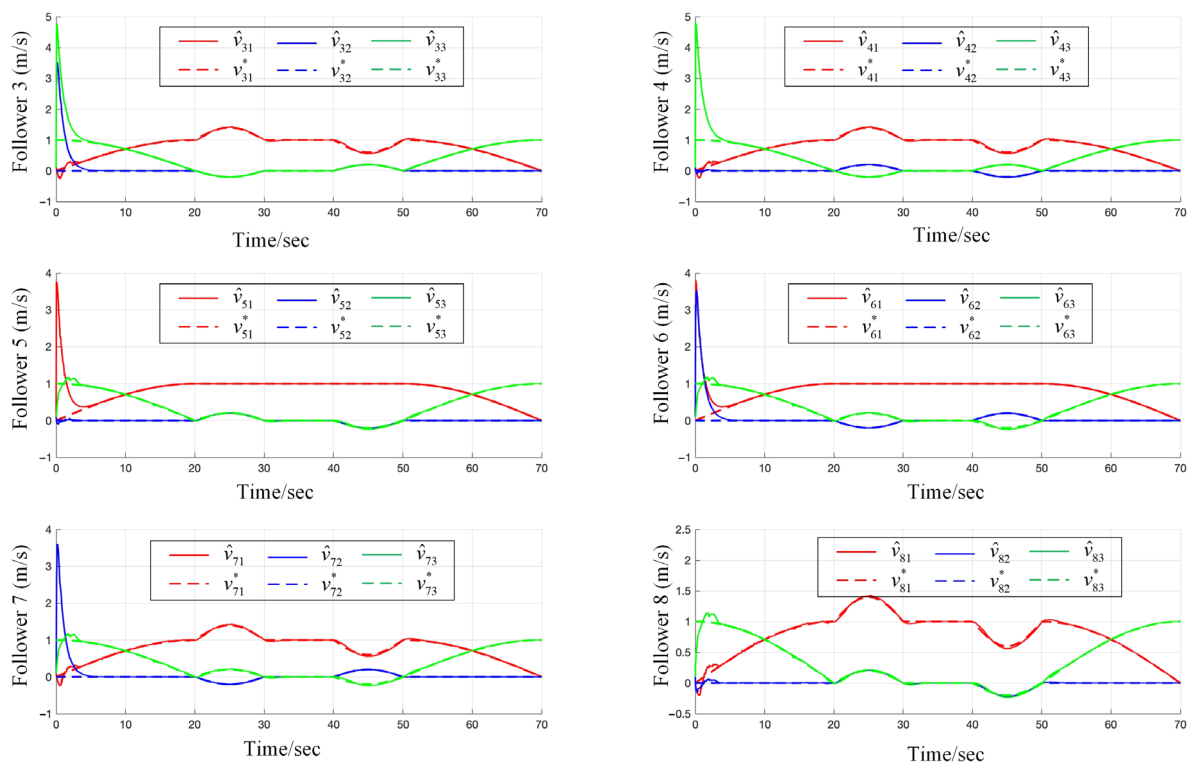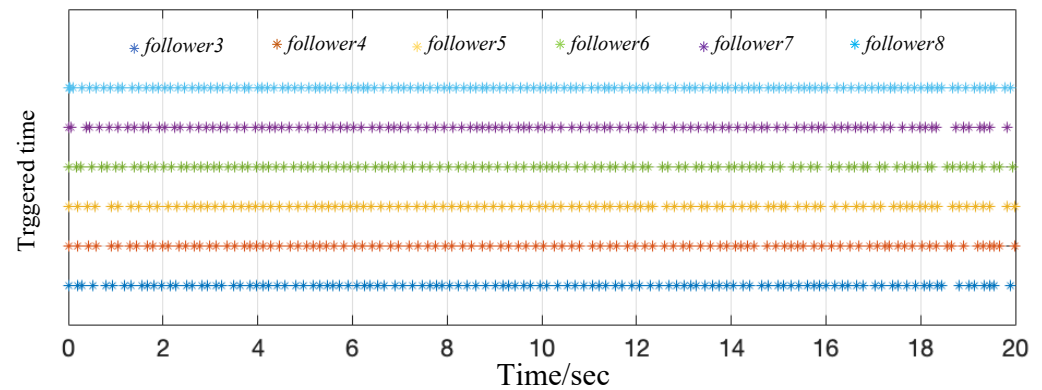

Figure 7. The velocity estimation effect of the follower UAVs.

Figure 8. The event-triggered time of the follower UAVs.
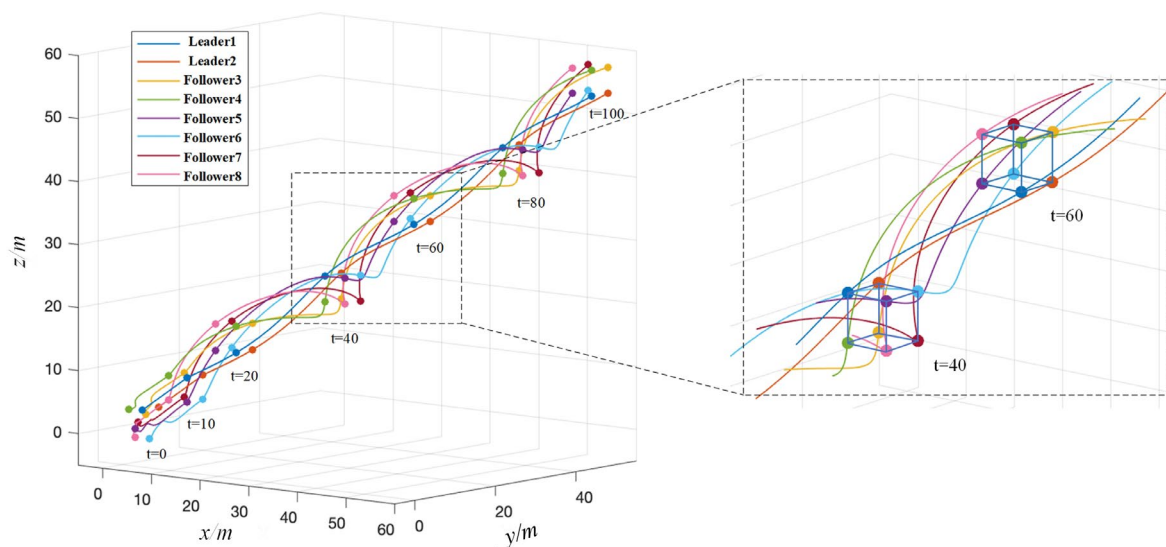
5.2. Rotation Formation Control for UAV

In this subsection, we evaluate the rotation effects of the UAV formation system through simulation experiments. the initial positions of the leader and the followers are the same as in Section 5.1 and the desired formation structure and the communication structure are also shown in Figure 2. The control parameters of the controller are selected as $k_v = 54$, $k_c = 2$, $a_1 = 5$, $a_2 = 0.3$, $c_1 = 1$, $c_2 = 0.07$. For $t \leq 10$, the leader's velocity was $v_1 = v_2 = \begin{bmatrix} 0.5 & 0.5 & 0.5 \end{bmatrix}^T$; otherwise, the velocity was as follows:

$$v_1 = v_2 = \begin{bmatrix} 0.05\pi \sin(0.05\pi(t-10)) + 0.5 & 0.5 & -0.05\pi \cos(0.05\pi(t-10)) + 0.5 \end{bmatrix}^T \quad (31)$$

The rotation matrix was as follows:

$$\begin{cases} R = \begin{bmatrix} \cos(0.05\pi(t-10)) & 0 & \sin(0.05\pi(t-10)) \\ 0 & 1 & 0 \\ -\sin(0.05\pi(t-10)) & 0 & \cos(0.05\pi(t-10)) \end{bmatrix}, t > 10 \\ R = \begin{bmatrix} 1 & 0 & 0 \\ 0 & 1 & 0 \\ 1 & 0 & 1 \end{bmatrix}, otherwise \end{cases} \quad (32)$$

The UAV formation system executes the rotation maneuver formation from 20 to 100 s, and the simulation results are shown in Figures 9–13.

Figure 9. The rotation formation control effects.
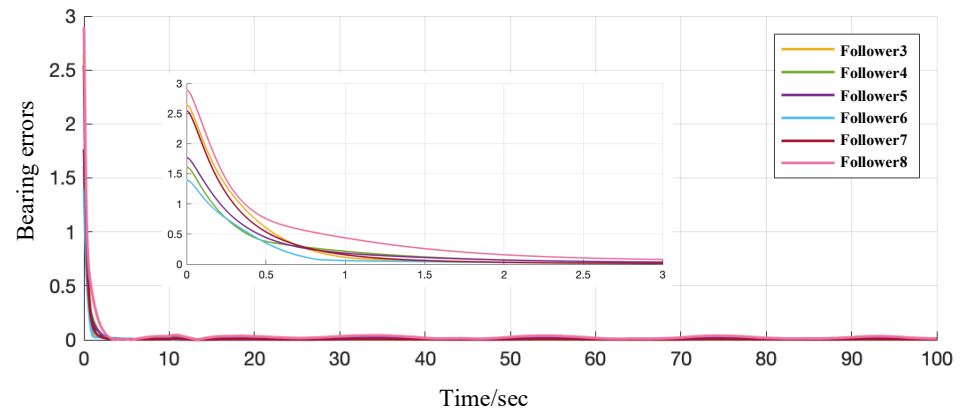
Figure 10. The bearing error $\sum\limits_{(i,j)\in\varepsilon} \|g_{ij} - g_{ij}^*\|$ of the follower UAVs.
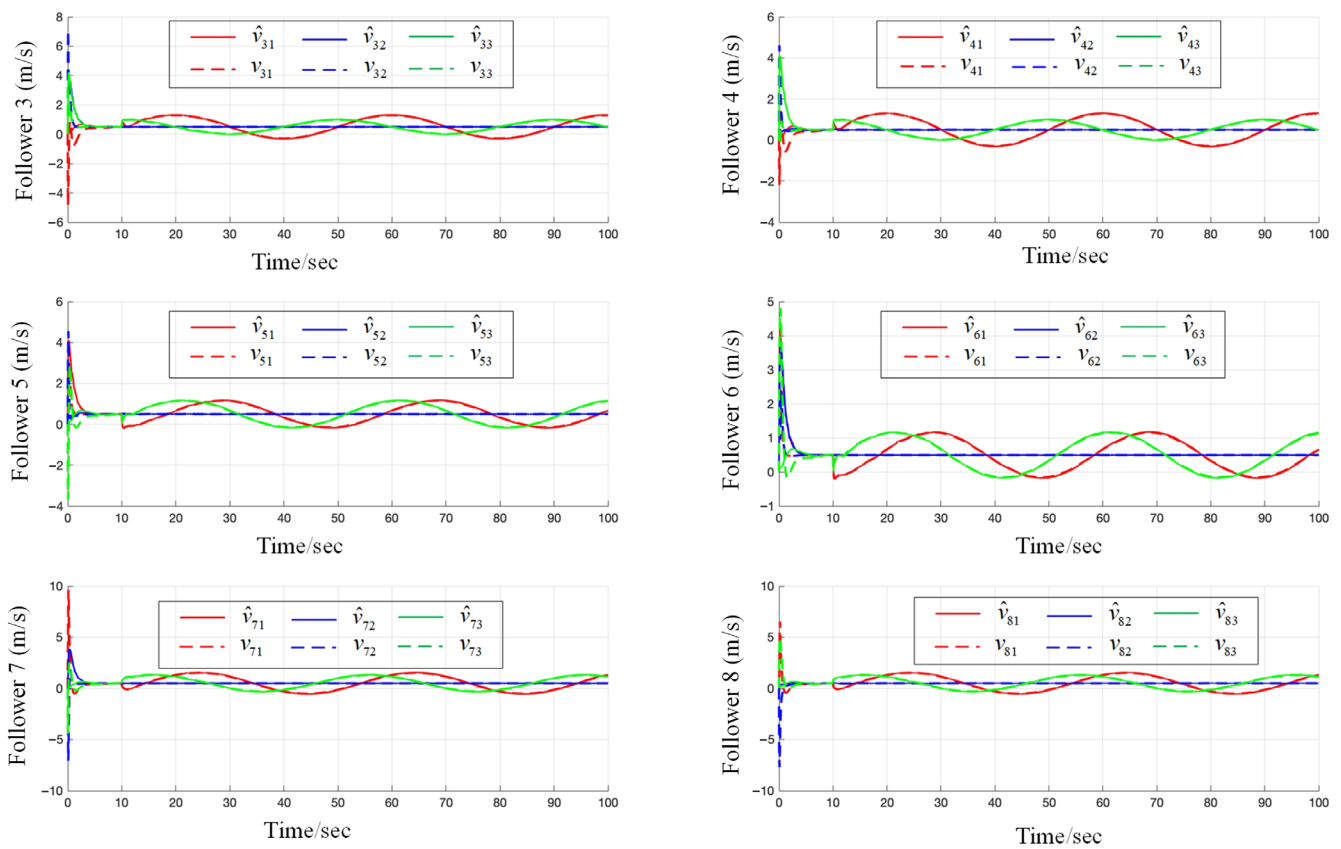
Figure 11. The velocity tracking effect of the follower UAVs.

From Figure 9, it is evident that the proposed distributed formation controller successfully achieves the intended rotation maneuver formations. As shown in Figures 10 and 11, the formation system adeptly follows the targeted relative bearing and velocity. Figure 12 demonstrates the effectiveness of the velocity observer designed in this study, accurately estimating the necessary formation velocity details. Figure 13 highlights the event-triggering instances for each follower UAV, indicating that communication takes place only when the triggering conditions are satisfied.

Figure 12. The velocity estimation effect of the follower UAVs.

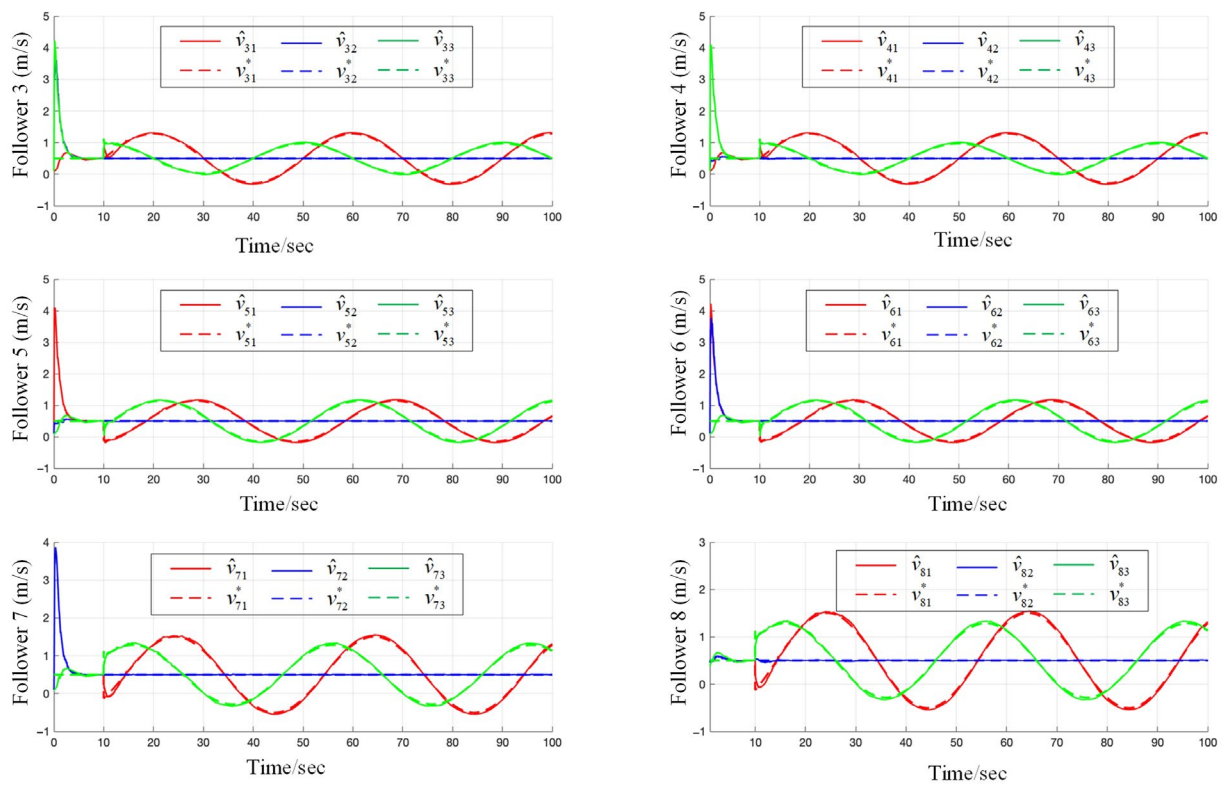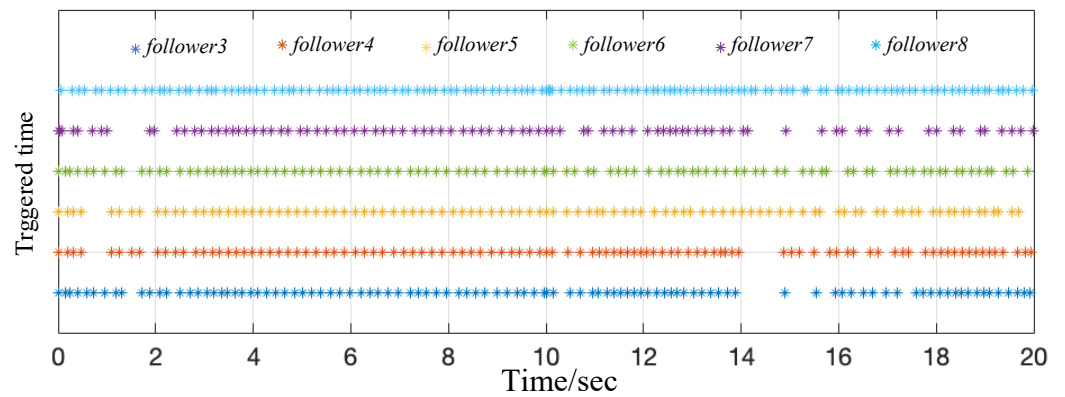**Figure 13.** The event-triggered time of the follower UAVs.

5.3. Comparative Simulation of Event-Triggering Strategies

This subsection verifies the effectiveness and superiority of the triggering strategies proposed in this paper by conducting comparative simulation experiments with traditional event triggering. To provide a clear comparison, to avoid repetition, the two traditional event-triggering strategies in this subsection are compared with the simulation results in Section 5.2. In these simulation experiments in this subsection, the initial states, controller parameters, and control objectives of the formation system remain the same as consistent with those in Section 5.2, and the only difference is the design of the event-triggering strategies. The triggering strategies used for comparison include both State-dependent Event-Triggered Strategies (SDETS) and Time-dependent Event-Triggered Strategies (TDETS). Lastly, the following are the specific forms of the two triggering strategies used for comparison:

$$\text{SDETS}: \ t_{k+1}^i = \inf\left\{t > t_k^i, d_i(t) > 0\right\}, i \in V_f \tag{33}$$

$$\text{TDETS}: \ t_{k+1}^i = \inf\left\{ t > t_k^i, \|\delta_i(t)\|^2 > v_1 e^{-v_2 t} \right\}, i \in V_f \qquad (34)$$

where $v_1 = 1$, $v_2 = 0.05$.

The simulation results for SDETS are illustrated in Figures 14 and 15, while those for TDETS are shown in Figures 16 and 17. To facilitate a comprehensive comparison, comparative results showing the number of event triggers and the minimum intervals for the three strategies are presented in Tables 1 and 2.
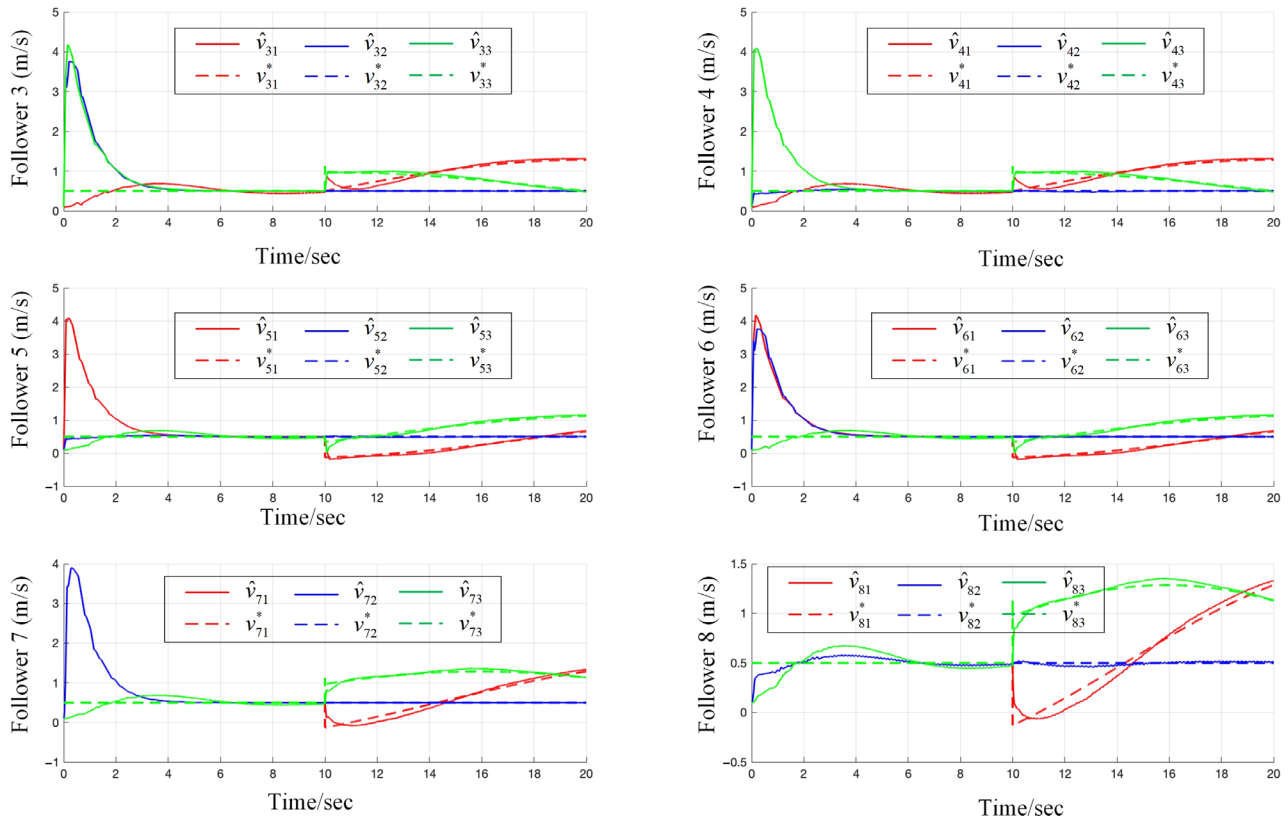
Figure 14. The velocity estimation effect of the follower UAVs based on the SDETS.
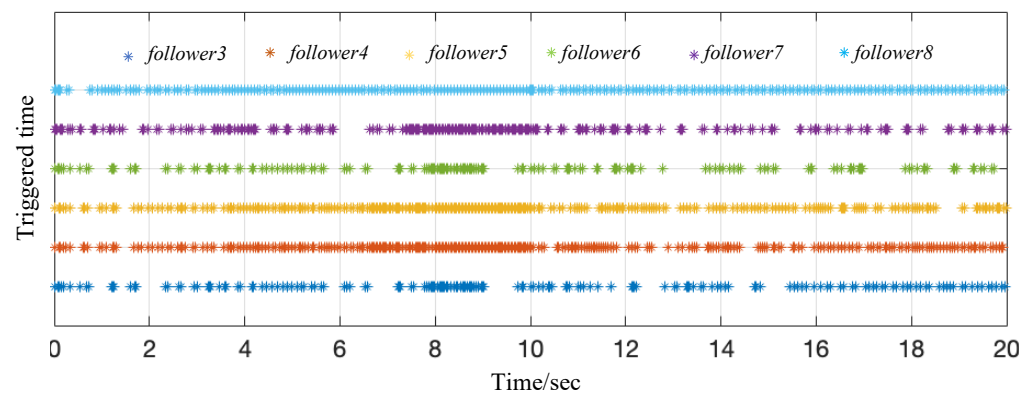
Figure 15. The event-triggered time of the follower UAVs based on the SDETS.
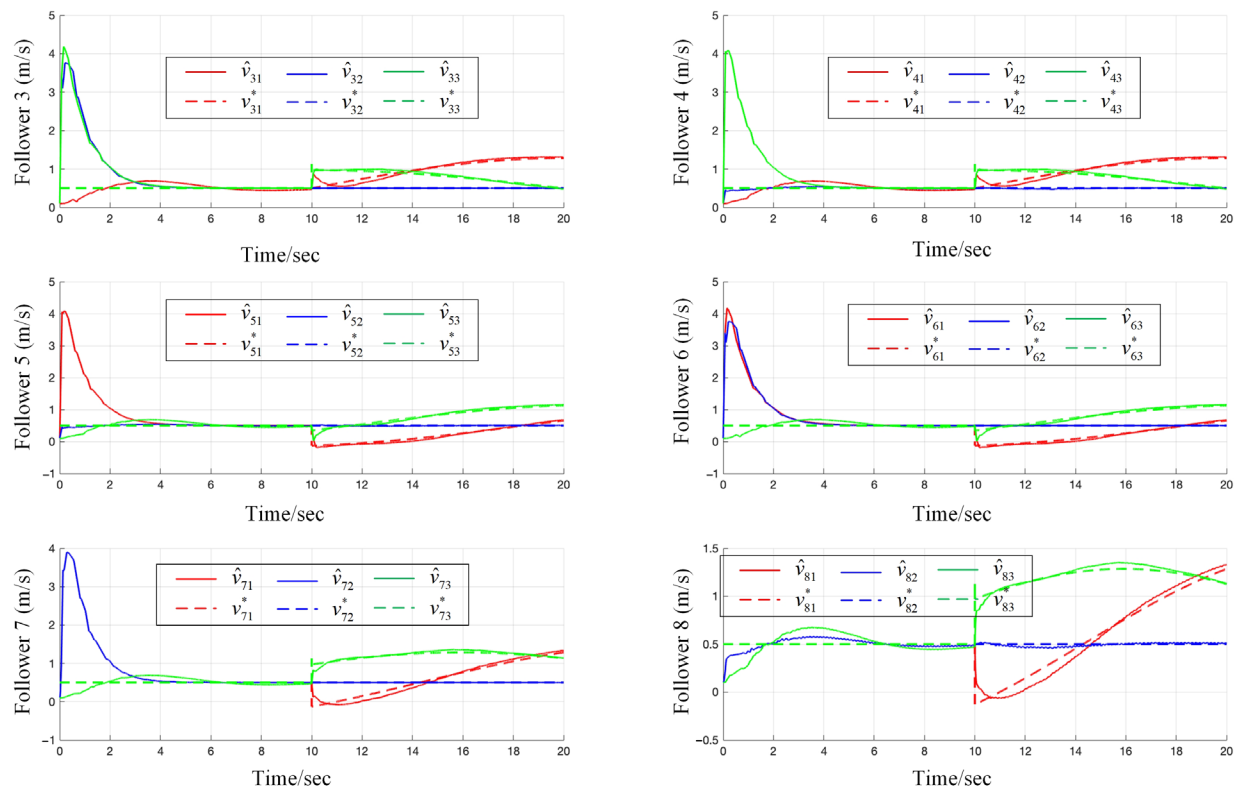
Figure 16. The velocity estimation effect of the follower UAVs based on the TDETS.
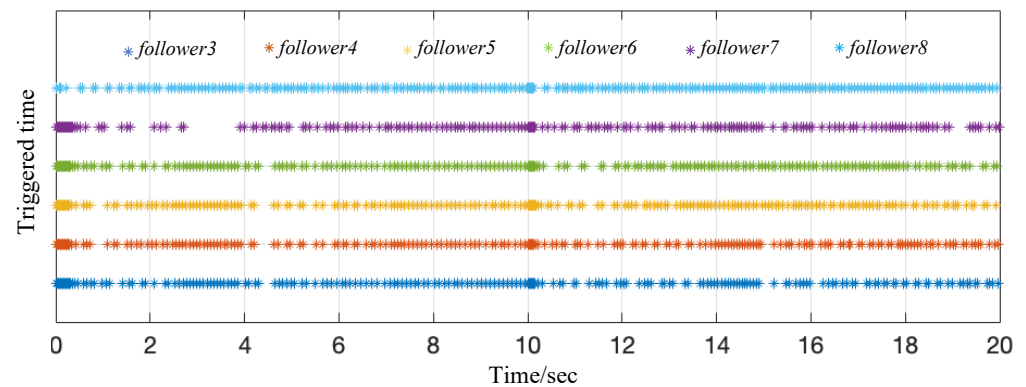
Figure 17. The event-triggered time of the follower UAVs based on the TDETS.

Table 1. Number of triggers for the three trigger strategies.

Tigger Times	Follower 3	Follower 4	Follower 5	Follower 6	Follower 7	Follower 8
DETS	180	167	162	170	161	220
SDETS	194	359	352	183	306	277
TDETS	224	225	250	235	212	273

Table 2. Minimum trigger interval for the three trigger strategies.

Interval Time	Follower 3	Follower 4	Follower 5	Follower 6	Follower 7	Follower 8
DETS	0.04 s	0.036 s	0.036 s	0.04 s	0.009 s	0.011 s
SDETS	0.004 s	0.005 s	0.005 s	0.004 s	0.001 s	0.009 s
TDETS	0.006 s	0.006 s	0.006 s	0.006 s	0.006 s	0.005 s

According to the results in Figure 12, Figure 14, and Figure 16, it is evident that all three triggering control strategies, combined with observers, can successfully estimate the desired speed. Observing from Figure 13, Figure 15, and Figure 16, it can be seen that the number of triggers in the dynamic event-triggering strategy (DETS) proposed in this chapter is significantly less than that of the traditional SDETS and TDETS, indicating a more efficient utilization of communication bandwidth and computational resources. Therefore, it can save communication bandwidth and computational resources more effectively. As evidenced by Tables 1 and 2, the triggering strategies proposed in this chapter demonstrate superior performance and are significantly better than the traditional event-triggering strategies in terms of the number of triggers and the minimum trigger interval time.

5.4. HITL Simulation

To comprehensively verify the performance and adaptability of the formation control algorithm, this section has established a Hardware-In-the-Loop (HITL) simulation platform to verify four different formation control effects: time-invariant formation, time-varying formation, formation scaling, and formation rotation. The structure of the HITL platform is shown in Figure 18.

Figure 18. The structure of the STIL platform.

In this section, four quadrotor drones are built in Gazebo, where UAV 1 and UAV 2 act as leaders, with the remaining two as follower drones. Figure 19 shows a photograph of the HITL platform, in which the ground station is utilized to display and record the drones' flight status and trajectories. The Gazebo simulation interface presents the actual flight paths of the drones, while the embedded computing platform is responsible for performing the computation tasks for the high-level formation control commands and issuing the control instructions. The formation structure and communication topology are shown in Figure 20.

To comprehensively verify the performance and adaptability of the formation control algorithm, this section investigates four different effects of formation control: time-invariant formation, time-varying formation, formation scaling, and formation rotation. By simulating UAVs executing complex formation tasks under conditions such as leader velocity changes, relative position adjustments, and desired changes in the relative direction of the formation, the aim is to emulate the variety of challenges faced by UAV formation in the real world. The experimental setup is as follows: Before the start of the simulation, all drones hover at a height of 15 m to ensure a unified starting point at the beginning of the experiment. This setup aims to simulate the preparation phase before the drone formation and provides a clear perspective for observation and analysis. To facilitate observation of the dynamic changes during the formation process, the entire formation will maintain the same altitude, that is, 15 m. At the beginning of the formation, the initial positions of the UAVs are: $p_1 = [3, 3, 15]^T m$, $p_2 = [3, 0, 15]^T m$, $p_3 = [-1, 5, 15]^T m$, $p_4 = [-1, -3, 15]^T m$,

The initial speeds of the follower drones are all zero. From 0 to 30 s, there is a constant speed tracking formation, and the speed of the leader UAVs are as follows:

$$\begin{cases} v_1 = \begin{bmatrix} 0.5 & 0 & 0 \end{bmatrix}^T, 0 \le t < 30 \\ v_2 = \begin{bmatrix} 0.5 & 0 & 0 \end{bmatrix}^T, 0 \le t \le 30 \end{cases} \tag{35}$$

Figure 19. Photograph of HITL simulation platform.

$$g_{12}^* = \begin{bmatrix} 0 & -1 & 0 \end{bmatrix}^T$$

$$g_{31}^* = \begin{bmatrix} 1 & 0 & 0 \end{bmatrix}^T$$

$$g_{32}^* = \begin{bmatrix} \sqrt{2}/2 & -\sqrt{2}/2 & 0 \end{bmatrix}^T$$

$$g_{43}^* = \begin{bmatrix} 0 & 1 & 0 \end{bmatrix}^T$$
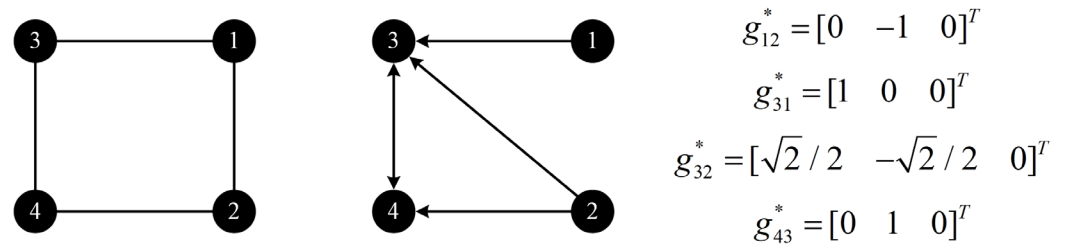
Figure 20. The target formation structure and communication topology structure.

From 30 to 90 s, it is a time-varying velocity tracking formation, and the velocity of the leader UAVs are as follows:

$$\begin{cases} v_1 = \begin{bmatrix} 0.2\pi \sin(0.02\pi(t-30)) & 0.2\pi \sin(0.02\pi(t-30)) & 0 \end{bmatrix}^T, 30 \le t < 90 \\ v_2 = \begin{bmatrix} 0.2\pi \sin(0.02\pi(t-30)) & 0.2\pi \sin(0.02\pi(t-30)) & 0 \end{bmatrix}^T, 30 \le t < 90 \end{cases} \tag{36}$$

From 100 to 150 s, it is a scaling maneuver formation, and the velocity of the leader UAVs are as follows:

$$\begin{cases} v_1 = \begin{bmatrix} 0.5 & \sin(0.05\pi(t-100))/\pi & 0 \end{bmatrix}^T, 100 \le t < 110 \\ v_1 = \begin{bmatrix} 0.5 & 0 & 0 \end{bmatrix}^T, 110 \le t < 140 \\ v_1 = \begin{bmatrix} 0.5 & -\sin(0.05\pi(t-140))/\pi & 0 \end{bmatrix}^T, 140 \le t < 150 \end{cases} \tag{37}$$

$$\begin{cases} v_2 = \begin{bmatrix} 0.5 & -\sin(0.05\pi(t-100))/\pi & 0 \end{bmatrix}^T, 100 \le t < 110 \\ v_2 = \begin{bmatrix} 0.5 & 0 & 0 \end{bmatrix}^T, 110 \le t < 140 \\ v_2 = \begin{bmatrix} 0.5 & \sin(0.05\pi(t-140))/\pi & 0 \end{bmatrix}^T, 140 \le t < 150 \end{cases} \tag{38}$$

From 100 to 150 s, it is a scaling maneuver formation, and the velocity of the leader UAVs are as follows:

$$\begin{cases} v_1 = \begin{bmatrix} 0.3\pi\cos(\pi(t-170)/40)/4 & 0.3\pi\sin(\pi(t-170)/40)/4 & 0 \end{bmatrix}^T, 170 \leq t < 210 \\ v_2 = \begin{bmatrix} 0.6\pi\cos(\pi(t-170)/40)/4 & 0.6\pi\sin(\pi(t-170)/40)/4 & 0 \end{bmatrix}^T, 170 \leq t < 210 \end{cases} \tag{39}$$

During the transition phase between different tasks, the speed of the leader UAVs are as follows:

$$\begin{cases} v_1 = \begin{bmatrix} 0.5 & 0 & 0 \end{bmatrix}^T, 90 \leq t < 100 \,\&\, 150 \leq t < 170 \\ v_2 = \begin{bmatrix} 0.5 & 0 & 0 \end{bmatrix}^T, 90 \leq t < 100 \,\&\, 150 \leq t < 170 \end{cases} \tag{40}$$

The rotation matrix of the system is as follows:

$$\begin{cases} R = \begin{bmatrix} \cos(\pi(t-170)/40) & \sin(\pi(t-170)/40) & 0 \\ -\sin(\pi(t-170)/40) & \cos(\pi(t-170)/40) & 0 \\ 0 & 0 & 1 \end{bmatrix}, t > 170 \\ R = \begin{bmatrix} 1 & 0 & 0 \\ 0 & 1 & 0 \\ 0 & 0 & 1 \end{bmatrix}, t \leq 170 \end{cases} \tag{41}$$

The parameters of the controller are chosen as: $k_c = 0.3$, $k_v = 5$, $a_1 = 5$, $a_2 = 0.3$, $c_1 = 1$, $c_2 = 0.01$, $c_3 = 150$, $c_4 = 1$. The simulation results are shown in Figures 21–25.
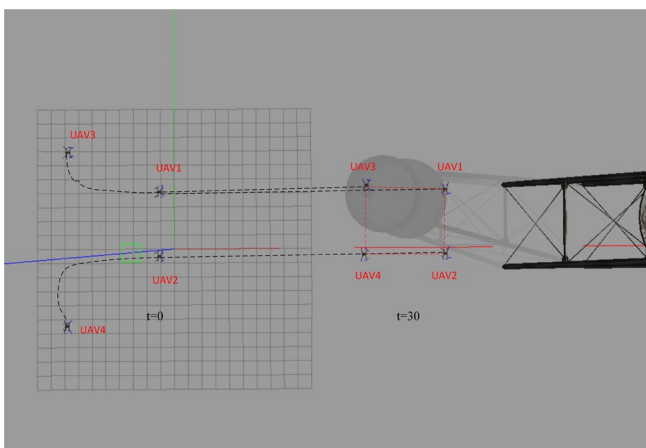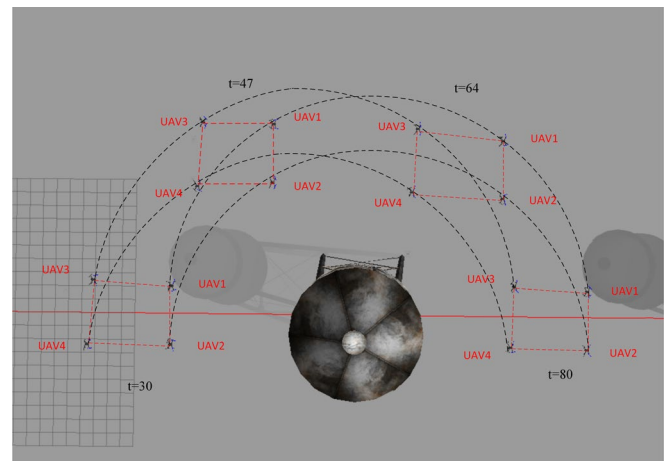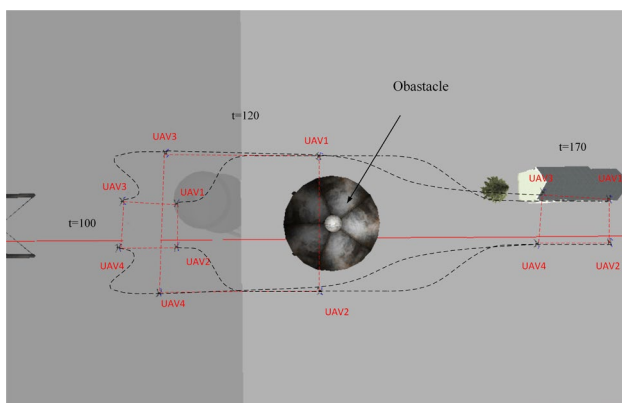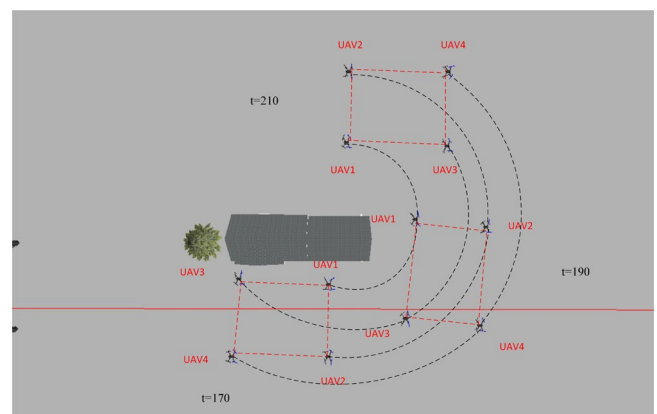
Figure 21. Control effects of HITL simulation platform. (**a**) Time-invariant formation; (**b**) Time-varying formation; (**c**) Scaling maneuver formation; (**d**) Rotation maneuver formation.
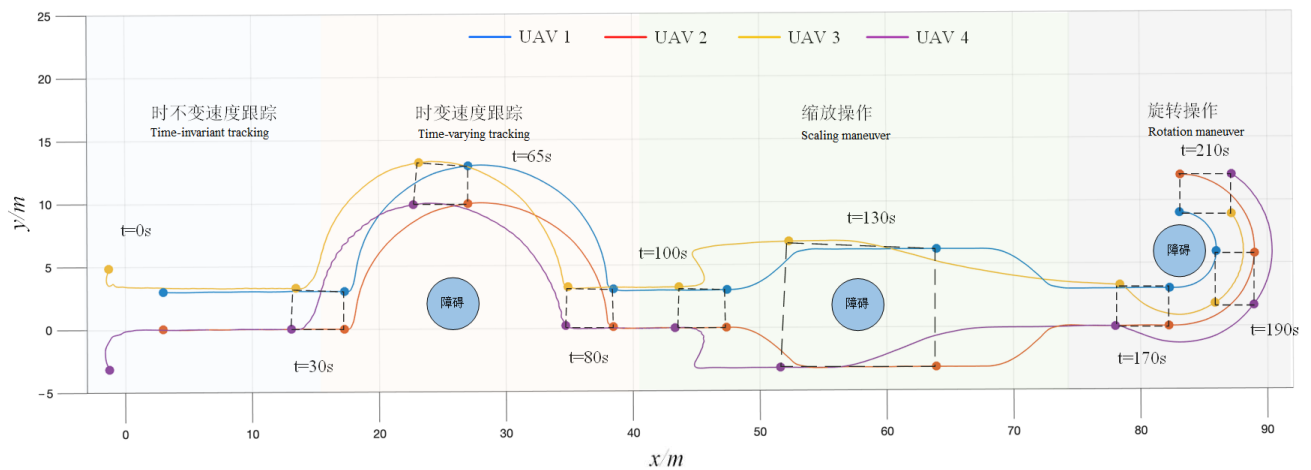
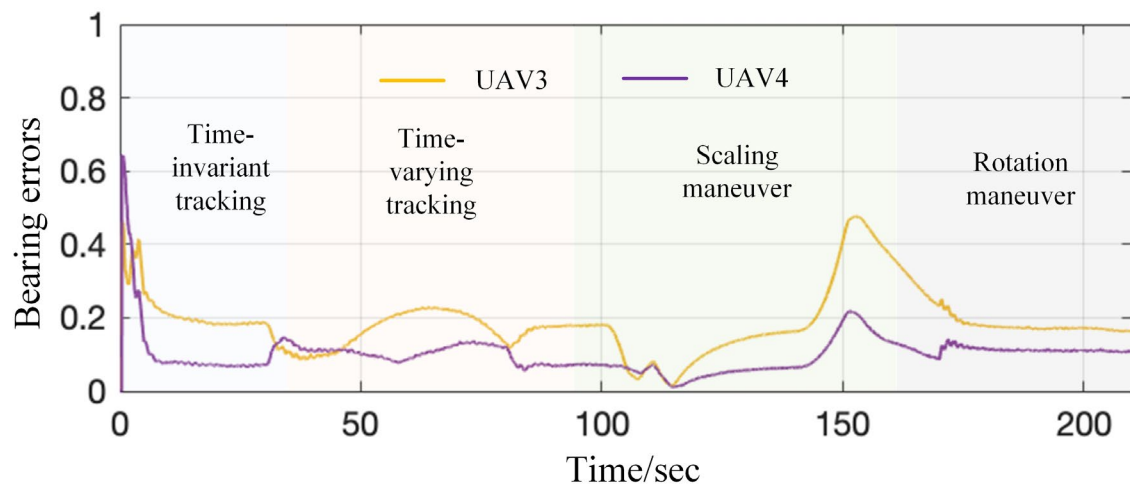**Figure 22.** Flight trajectory under HITL simulation platform.

Figure 23. Bearing errors of follower UAVs.

Figure 21 demonstrates the simulation results in the Gazebo simulation environment, specifically illustrating four different control tasks: time-invariant tracking, time-varying tracking, scaling maneuver, and rotation maneuver. The dashed lines clearly mark the flight trajectories of UAVs during each task, showcasing the precision and reliability of the formation control algorithm in maintaining formation structure. Following this, Figure 22 shows UAV flight trajectories based on real flight test data, further validating the algorithm's effectiveness in practical applications. Figure 23 focuses on the relative orientation errors during various tasks, indicating effective convergence towards minimal error, demonstrating the system's capability to maintain formation and orientation. Figure 24 analyzes the performance of distributed velocity observers by showing how the estimators accurately track the desired velocities, highlighting the observer design's effectiveness in dynamic conditions. Lastly, Figure 25 presents the event-triggering moments of the velocity observers, showcasing how a well-designed event-triggering mechanism can ensure communication efficiency while significantly reducing bandwidth and resource consumption.
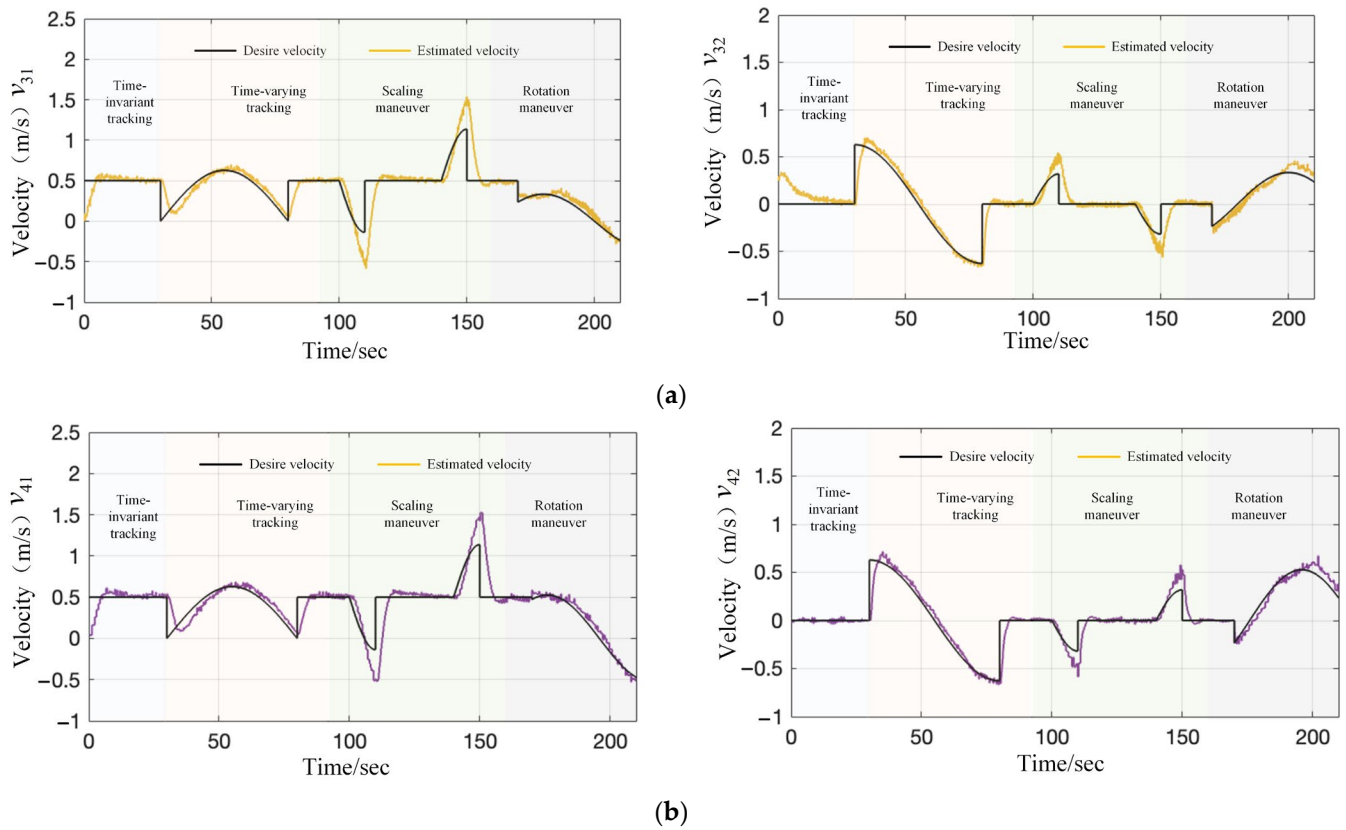
Figure 24. The velocity estimation effect of follower UAV. (**a**) The velocity estimation effect of follower UAV 3; (**b**) The velocity estimation effect of follower UAV 4.
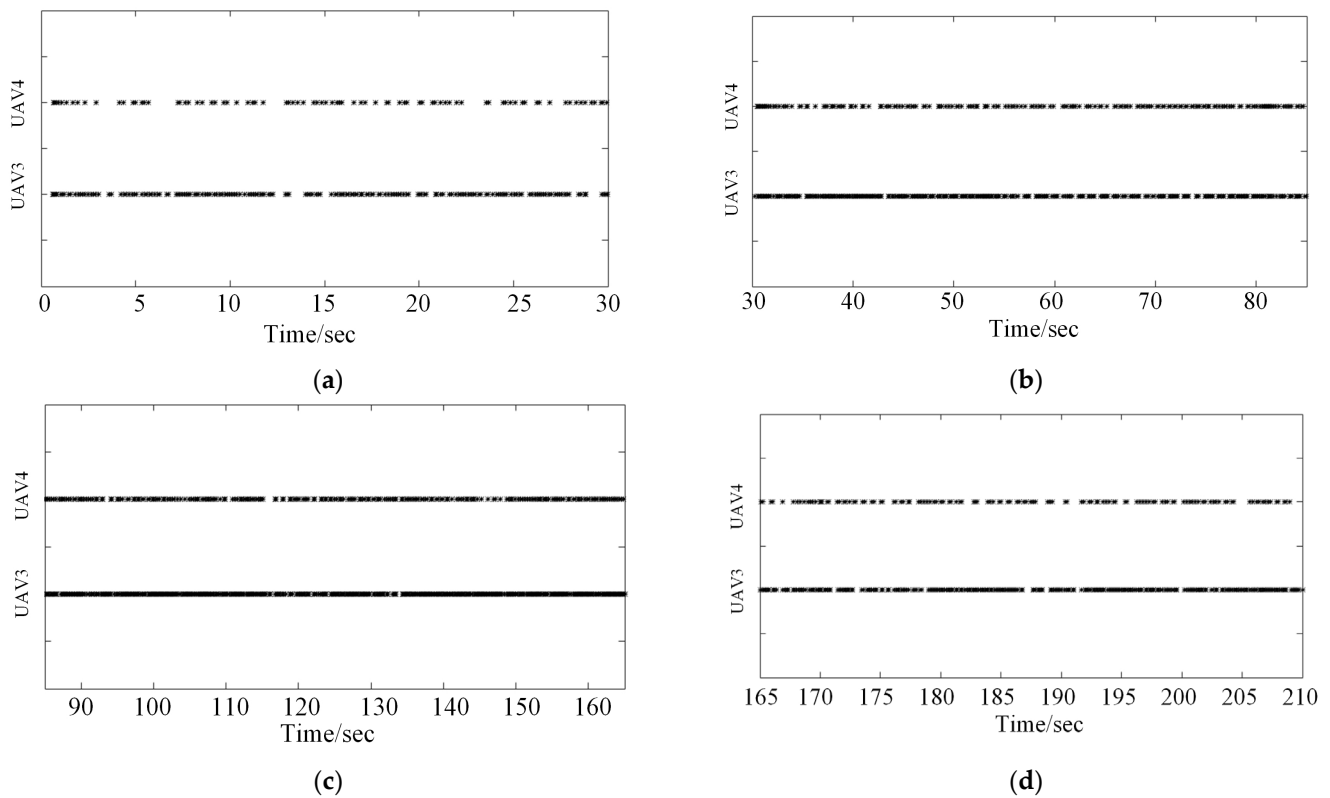
Figure 25. The triggered instants under four types of tasks. (**a**) Time-invariant tracking; (**b**) Time-varying tracking; (**c**) Scaling maneuver; (**d**) Rotation maneuver.

6. Conclusions

This study delves into the intricate realm of leader-following formation maneuver control issues associated with UAVs, incorporating elements such as time-varying velocity and time-varying relative bearing. In our investigation, we introduced an event-triggered bearing-based distributed velocity observer that relies exclusively on the intended position and velocity data of leader UAVs. Our event-triggered mechanism is notable for its capability to significantly reduce the continuous communication needs between UAVs, thereby playing a pivotal role in conserving both communication bandwidth and vital resources. Merging the event-triggered velocity observer with the backstepping control technique, we present a bearing-only formation maneuver control strategy. In validating our proposed approach, we conducted extensive numerical simulations and HITL simulations. These tests clearly showed the method's prowess in achieving formation maneuver control objectives, encompassing translation, scaling, and rotation control.

Appendix A

Appendix A.1. Proof of Theorem 1

Proof of Theorem 1. First, let us define matrix $F = \begin{bmatrix} a_3 I_{dn_f} & M_{ff} \\ M_{ff} & B_{ff} \end{bmatrix}$ wherein a_3 is positive constant. Given that B_{ff} is positive, the Schur complement of the matrix F can be written as $a_3 I_{dn_f} - a_2^2 M_{ff} B_{ff}^{-1} M_{ff}$. If a_3 satisfies condition (16c), then $a_3 I_{dn_f} > \lambda_m \left(a_2^2 M_{ff} B_{ff}^{-1} M_{ff} \right) I_{dn_f} \geq a_2^2 M_{ff} B_{ff}^{-1} M_{ff}$, which means $a_3 I_{dn_f} - a_2^2 M_{ff} B_{ff}^{-1} M_{ff} > 0$. Consequently, based on Lemma 1, matrix F is positive definite.

Consider the following Lyapunov candidate function

$$V_1 = \frac{1}{2} col^T(\widetilde{p}_f, \widetilde{v}_f) F col(\widetilde{p}_f, \widetilde{v}_f) \tag{A1}$$

The derivate of V_1 is given as follows:

$$\dot{V}_1 = \widetilde{v}_f^T \left(M_{ff} + \frac{1}{2} \dot{B}_{ff} \right) \widetilde{v}_f + \widetilde{p}_f^T \left(\dot{M}_{ff} + a_3 I_{dn_f} \right) \widetilde{v}_f + \left(\widetilde{v}_f^T B_{ff} + \widetilde{p}_f^T M_{ff} \right) \dot{\widetilde{v}}_f \tag{A2}$$

According to the equation distributed observer (15), the above equation can be rewritten as follows:

$$\begin{aligned} \dot{V}_1 &= -\widetilde{v}_f^T \left(a_1 B_{ff}^2 - M_{ff} - \frac{1}{2} \dot{B}_{ff} \right) \widetilde{v}_f - \widetilde{p}_f^T \left(2a_1 M_{ff} B_{ff} - \dot{M}_{ff} - a_3 I_{dn_f} \right) \widetilde{v}_f - \widetilde{p}_f^T \left(a_1 M_{ff}^2 \right) \widetilde{p}_f \\ &\quad - a_1 \left(\widetilde{v}_f^T B_{ff} + \widetilde{p}_f^T M_{ff} \right) \left(\left(B_{ff} e_f + M_{ff} z_f \right) + \left(B_{fl} e_l + M_{fl} z_l \right) \right) \\ &= -col^T(\widetilde{v}_f, \widetilde{p}_f) U col(\widetilde{v}_f, \widetilde{p}_f) - Y \end{aligned} \tag{A3}$$

where

$$U = \begin{bmatrix} a_1 M_{ff}^2 & a_1 M_{ff} B_{ff} - \frac{1}{2}(\dot{M}_{ff} + a_3 I_{dn_f}) \\ a_1 M_{ff} B_{ff} - \frac{1}{2}(\dot{M}_{ff} + a_3 I_{dn_f}) & a_1 B_{ff}^2 - M_{ff} - \frac{1}{2}\dot{B}_{ff} \end{bmatrix},$$

$$Y = a_1 \left(\tilde{v}_f^T B_{ff} + \tilde{p}_f^T M_{ff} \right) \left(\left(B_{ff} e_f + M_{ff} z_f \right) + \left(B_{fl} e_l + M_{fl} z_l \right) \right).$$

According to condition (16b), we can know that the matrix M_{ff} and M_{ff}^2 are positive definite. If the constant a_1 satisfies Condition (16a), the matrix $a_1 B_{ff}^2 - M_{ff} - \frac{1}{2}\dot{B}_{ff}$ is positive definite. Moreover, if the Condition (16a) to (16c) hold, the matrix U is positive definite. According to Lemma 3, we have the follows:

$$\dot{V}_1 \le -\frac{1}{2}\lambda_{\min}(M_1)\tilde{p}_f^T \tilde{p}_f - \frac{1}{2}\lambda_{\min}(M_2)\tilde{v}_f^T \tilde{v}_f - Y \tag{A4}$$

According to Young's inequality, the above inequality can be rewritten as

$$
\begin{aligned}
\dot{V}_1 \le {}& -\frac{1}{2}\sum_{i=n_l+1}^{n}\lambda_{\min}(M_1)\|\tilde{p}_i\|^2 - \frac{1}{2}\sum_{i=n_l+1}^{n}\lambda_{\min}(M_2)\|\tilde{v}_i\|^2 + \frac{1}{2}\lambda_{\max}^2\left(B_{ff}\right)\|\tilde{v}_f\|^2 \\
&+ \frac{a_1^2}{2}\|B_{ff}e_f + B_{fl}e_l\|^2 + \frac{1}{2}\lambda_{\max}^2\left(M_{ff}\right)\|\tilde{p}_f\|^2 + \frac{a_1^2}{2}\|M_{ff}z_f + M_{fl}z_l\|^2 \\
\le {}& -\frac{1}{2}\left(\lambda_{\min}(M_1) - \lambda_{\max}^2\left(M_{ff}\right)\right)\sum_{i=n_l+1}^{n}\|\tilde{p}_i\|^2 - \frac{1}{2}\left(\lambda_{\min}(M_2) - \lambda_{\max}^2\left(B_{ff}\right)\right)\sum_{i=n_l+1}^{n}\|\tilde{v}_i\|^2 \\
&+ \frac{a_1^2}{2}\sum_{i=n_l+1}^{n}\sum_{j\in N_i}\|B_{ij}e_i\| + \frac{a_1^2}{2}\sum_{i=n_l+1}^{n}\sum_{j\in N_i}\|B_{ij}e_j\| + \frac{a_1^2}{2}\sum_{i=n_l+1}^{n}\sum_{j\in N_i}\|M_{ij}z_i\| + \frac{a_1^2}{2}\sum_{i=n_l+1}^{n}\sum_{j\in N_i}\|M_{ij}z_j\|
\end{aligned} \tag{A5}
$$

Since the graph is undirected, we have

$$\frac{a_1^2}{2}\sum_{i=n_l+1}^{n}\sum_{j\in N_i}\|B_{ij}e_i\| + \frac{a_1^2}{2}\sum_{i=n_l+1}^{n}\sum_{j\in N_i}\|B_{ij}e_j\| = a_1^2\sum_{i=n_l+1}^{n}\sum_{j\in V_f}\|B_{ij}e_i\| + \frac{a_1^2}{2}\sum_{i=n_l+1}^{n}\sum_{j\in V_l}\|B_{ij}e_j\| \tag{A6}$$

$$\frac{a_1^2}{2}\sum_{i=n_l+1}^{n}\sum_{j\in N_i}\|M_{ij}z_i\| + \frac{a_1^2}{2}\sum_{i=n_l+1}^{n}\sum_{j\in N_i}\|M_{ij}z_j\| = a_1^2\sum_{i=n_l+1}^{n}\sum_{j\in V_f}\|M_{ij}z_i\| + \frac{a_1^2}{2}\sum_{i=n_l+1}^{n}\sum_{j\in V_l}\|M_{ij}z_j\| \tag{A7}$$

Substituting Equations (A6) and (A7) into (A5) yields:

$$
\begin{aligned}
\dot{V}_1 \le {}& -\frac{1}{2}\left(\lambda_{\min}(M_1) - \lambda_{\max}^2\left(M_{ff}\right)\right)\sum_{i=n_l+1}^{n}\|\tilde{p}_i\|^2 - \frac{1}{2}\left(\lambda_{\min}(M_2) - \lambda_{\max}^2\left(B_{ff}\right)\right)\sum_{i=n_l+1}^{n}\|\tilde{v}_i\|^2 \\
&+ a_1^2\sum_{i=n_l+1}^{n}\left(\sum_{j\in V_f}\left(\|B_{ij}e_i\|^2 + \|M_{ij}z_i\|^2\right) + \frac{1}{2}\sum_{j\in V_l}\left(\|B_{ij}e_j\|^2 + \|M_{ij}z_j\|^2\right)\right) \\
= {}& -\frac{1}{2}\left(\lambda_{\min}(M_1) - \lambda_{\max}^2\left(M_{ff}\right)\right)\sum_{i=n_l+1}^{n}\|\tilde{p}_i\|^2 - \frac{1}{2}\left(\lambda_{\min}(M_2) - \lambda_{\max}^2\left(B_{ff}\right)\right)\sum_{i=n_l+1}^{n}\|\tilde{v}_i\|^2 + a_1^2\sum_{i=n_l+1}^{n}\delta_i
\end{aligned} \tag{A8}
$$

Then we define the following function

$$V_2 = \sum_{i=n_l+1}^{n}\alpha_i(t) \tag{A9}$$

According to (13) and (14), it follows that

$$\dot{\alpha}_i > \left(c_2 - \frac{c_3}{c_4}\right)\alpha_i \tag{A10}$$

From the comparison theorem [42] it is clear that that $\alpha_i(t) > 0, t \in [0, \infty)$, therefore V_2 is a Lyapunov candidate function.

Derivation of V_2 yields

$$\dot{V}_2 = -\sum_{i=n_l+1}(c_2\alpha_i + c_3 d_i) = -\sum_{i=n_l+1}\left(c_2\alpha_i + c_3\|\delta_i\|^2 - c_1 c_3\|\overline{m}_i\|^2\right) \tag{A11}$$

According to (5), we have

$$
\begin{aligned}
\sum_{i=n_l+1}\|\overline{m}_i\|^2 &= a_1^2 \sum_{i=n_l+1}\left(\|\sum_{j\in N_i}B_{ij}(e_i - e_j + \widetilde{v}_i - \widetilde{v}_j) + \sum_{j\in N_i}M_{ij}(z_i - z_j + \widetilde{p}_i - \widetilde{p}_j)\|^2\right) \\
&\leq 2a_1^2 \sum_{i=n_l+1}\delta_i + 2a_1^2\lambda_1 n_f \sum_{i=n_l+1}\|\widetilde{v}_i\|^2 + 2a_1^2\lambda_2 n_f \sum_{i=n_l+1}\|\widetilde{p}_i\|^2
\end{aligned}
\tag{A12}
$$

where

$$\lambda_1 = \max_{i\in V_f,(i,j)\in\varepsilon}\left\{\lambda_{\max}(B_{ij})\right\}, \ \lambda_2 = \max_{i\in V_f,(i,j)\in\varepsilon}\left\{\lambda_{\max}(M_{ij})\right\}.$$

Substituting (A12) into (A11) yields

$$\dot{V}_2 \leq -c_2\sum_{i=n_l+1}\alpha_i - c_3\left(1 - 2a_1^2 c_1\right)\sum_{i=n_l+1}\delta_i + 2a_1^2 c_1 c_3\lambda_1 n_f \sum_{i=n_l+1}\|\widetilde{v}_i\|^2 + 2a_1^2 c_1 c_3\lambda_2 n_f \sum_{i=n_l+1}\|\widetilde{p}_i\|^2 \tag{A13}$$

Let $V = V_1 + V_2$, and combining (A8) and (A11), the derivation of V yields

$$\dot{V} = \left(3a_1^2 - c_3\left(1 - 2a_1^2 c_1\right)\right)\sum_{i=n_l+1}^{n}\delta_i - c_2\sum_{i=n_l+1}\alpha_i - \frac{1}{2}\theta_1\sum_{i=n_l+1}^{n}\|\widetilde{p}_i\|^2 - \frac{1}{2}\theta_2\sum_{i=n_l+1}^{n}\|\widetilde{v}_i\|^2 \tag{A14}$$

Let $c_3 = 3a_1^2/(1 - 2a_1^2 c_1) > 0$, then the above inequality can be written as

$$\dot{V} \leq -\varepsilon V \tag{A15}$$

where $\varepsilon = \min\{\theta_1/\lambda_{\max}(F), \theta_2/\lambda_{\max}(F), c_2\}$.
From condition (16d), ε is a positive constant.
Solving Inequality (A15) gives

$$V(t) \leq V(0)e^{-\varepsilon t} \tag{A16}$$

It follows from Lyapunov theorem that the estimation errors $\widetilde{p}_i$ and $\widetilde{v}_i$ of the system converge exponentially to zero.

Next, we prove that the Zeno behavior of the formation system can be excluded. First, the stability analysis above demonstrates that the estimation errors for $\widetilde{p}_i$ and $\widetilde{v}_i$ are bounded. Consequently, each e_i and z_i is also bounded. Specifically, there exists a positive constant K such that $d\|e_i\|/dt \leq K$ and $d\|z_i\|/dt \leq K$ for $t \geq 0$. Thus, the derivative of $\|e_i\|$ on (t_k^i, t_{k+1}^i) satisfies:

$$d\|d_i(t)\|/dt \leq 2|N_i|\lambda_i K \tag{A17}$$

where $\lambda_{3i} = \max_{j\in N_i}\{\lambda_{\max}(B_{ij}), \lambda_{\max}(M_{ij})\}$, $|N_i|$ is the number of neighboring UAV of UAV i.

Since $\lim_{t\to t_{k+1}^i} d_i(t) = 0$, we have $\|d_i(t)\| \leq 2|N_i|\lambda_{3i}K(t - t_k^i)$ for all $t \in (t_k^i, t_{k+1}^i]$. According to (13) and (14), we have $\alpha_i(t) \geq \alpha_i(0)e^{(c_2 - c_3/c_4)t} > 0$.

When $t = t_{k+1}^i$, based on (14), the following inequalities hold:

$$\alpha_i(0)e^{(c_2 - c_3/c_4)t}/c_4 < \|d_i(t)\| \leq 2|N_i|\lambda_{3i}K(t_{k+1}^i - t_k^i) \tag{A18}$$

The above inequality implies the following:

$$(t_{k+1}^i - t_k^i) > \frac{\alpha_i(0)e^{(c_2 - c_3/c_4)t}}{2|N_i|\lambda_{3i}Kc_4} > 0 \tag{A19}$$

which means the Zeno behavior can be effectively avoided. This completes the proof of Theorem 1. □

Appendix A.2. Proof of Theorem 2

Proof of the Theorem 2. Substituting control law (26) into (25), we obtain the following:

$$
\begin{aligned}
\dot{V}_3 &= -k_c s^T s - k_v \widetilde{g}^T \overline{R R} \widetilde{g} + \widetilde{g}^T \overline{R} \hat{v} + \widetilde{g}^T \dot{g}^* \\
&\leq -k_c \|s\|^2 - k_v \lambda_{\min}(\overline{R}^T \overline{R}) \|\widetilde{g}\| + \widetilde{g}^T \overline{R} \hat{v} + \widetilde{g}^T \dot{g}
\end{aligned}
\tag{A20}
$$

According to the Young's inequality, we have the following:

$$
\begin{aligned}
\widetilde{g}^T \overline{R} \hat{v} &\leq \tfrac{1}{2} \lambda_{\max}(\overline{R}) \|\widetilde{g}\|^2 + \tfrac{1}{2} \lambda_{\max}(\overline{R}) \|\hat{v}\|^2 \\
\widetilde{g}^T \dot{g}^* &\leq \tfrac{1}{2} \|\widetilde{g}\|^2 + \tfrac{1}{2} \|\dot{g}^*\|^2
\end{aligned}
\tag{A21}
$$

Substituting the above inequality into (A20), we obtain the following:

$$
\dot{V}_3 \leq -k_c \|s\|^2 - \left(k_v \lambda_{\min}(\overline{R}^T \overline{R}) - \frac{1}{2} \lambda_{\max}(\overline{R}) - \frac{1}{2} \right) \|\widetilde{g}\|^2 + \delta
\tag{A22}
$$

where $\delta = \frac{1}{2} \lambda_{\max}(\overline{R}) \|\hat{v}\| + \frac{1}{2} \|\dot{g}^*\|$.

According to Theorem 1 and Assumption 2, we know that the $\hat{v}$ and $\dot{g}^*$ are bounded, which means δ is bounded and has the upper value $\delta_m > 0$. Let $\kappa = \max\left\{ k_c, k_v \lambda_{\min}(\overline{R}^T \overline{R}) - \frac{1}{2} \lambda_{\max}(\overline{R}) - \frac{1}{2} \right\}$, (A22) can be rewritten as follows:

$$
\dot{V}_3 \leq -2\kappa V_3 + \delta_m
\tag{A23}
$$

By solving the above inequality, we have the following:

$$
0 \leq V_3 \leq \frac{\delta_m}{2\kappa} + \left(V_3(0) - \frac{\delta_m}{2\kappa} \right) e^{-2\kappa t}
\tag{A24}
$$

Based on Inequality (A24), it is evident that the Lyapunov function $V_3(t)$ is bounded by $\delta_m/2\kappa$. Consequently, the bearing error $\widetilde{g}$ and velocity tracking error v^e are uniformly ultimately bounded (UUB). It is worth noting that by increasing the control parameters k_c and k_v, the upper bound $\delta_m/2\kappa$ can be reduced. This implies that the bearing errors $\widetilde{g}$ and velocity tracking error v^e can be made to converge to a compact set around zero. As Theorem 1 has established that $\lim_{t \to \infty} \widetilde{v} \to 0$, it can be concluded that $v - v^* = v^e - \widetilde{v}$ is also UUB and can converge to a compact set around zero. This completes the proof of Theorem 2. □

References

1. Yan, Z.; Han, L.; Li, X.; Dong, X.; Li, Q.; Ren, Z. Event-triggered formation control for time-delayed discrete-time multi-agent system applied to multi-UAV formation flying. *J. Frankl. Inst.* **2023**, *360*, 3677–3699. [CrossRef]
2. Mohsan SA, H.; Khan, M.A.; Noor, F.; Ullah, I.; Alsharif, M.H. Towards the unmanned aerial vehicles (UAVs): A comprehensive review. *Drones* **2022**, *6*, 147. [CrossRef]
3. Su, J.; Zhu, X.; Li, S.; Chen, W.-H. AI meets UAVs: A survey on AI empowered UAV perception systems for precision agriculture. *Neurocomputing* **2022**, *518*, 242–270. [CrossRef]
4. Zhang, M.; Li, W.; Wang, M.; Li, S.; Li, B. Helicopter–UAVs search and rescue task allocation considering UAVs operating environment and performance. *Comput. Ind. Eng.* **2022**, *167*, 107994. [CrossRef]
5. Mekdad, Y.; Aris, A.; Babun, L.; El Fergougui, A.; Conti, M.; Lazzeretti, R.; Uluagac, A.S. A survey on security and privacy issues of UAVs. *Comput. Netw.* **2023**, *224*, 109626. [CrossRef]
6. Ouyang, Q.; Wu, Z.; Cong, Y.; Wang, Z. Formation control of unmanned aerial vehicle swarms: A comprehensive review. *Asian J. Control.* **2023**, *25*, 570–593. [CrossRef]

7. Yasin, J.N.; Mohamed, S.A.; Haghbayan, M.H.; Heikkonen, J.; Tenhunen, H.; Plosila, J. Unmanned aerial vehicles (uavs): Collision avoidance systems and approaches. *IEEE Access* **2020**, *8*, 105139–105155. [CrossRef]

8. Zhang, R.; Cao, S.; Zhao, K.; Yu, H.; Hu, Y. A hybrid-driven optimization framework for fixed-wing uav maneuvering flight planning. *Electronics* **2021**, *10*, 2330. [CrossRef]

9. Huang, S.; Teo, R.S.H.; Tan, K.K. Collision avoidance of multi unmanned aerial vehicles: A review. *Annu. Rev. Control.* **2019**, *48*, 147–164. [CrossRef]

10. Qin, B.; Fan, Y.; Xiao, T.; Li, Z. Distributed type-2 fuzzy adaptive control for heterogeneous nonlinear multiagent systems. *Asian J. Control.* **2022**, *24*, 1755–1768. [CrossRef]

11. Cheng, S.; Dong, H.; Yu, L.; Zhang, D.; Ji, J. Consensus of second-order multi-agent systems with directed networks using relative position measurements only. *Int. J. Control. Autom. Syst.* **2019**, *17*, 85–93. [CrossRef]

12. Shalaby, M.; Cossette, C.C.; Forbes, J.R.; Le Ny, J. Relative position estimation in multi-agent systems using attitude-coupled range measurements. *IEEE Robot. Autom. Lett.* **2021**, *6*, 4955–4961. [CrossRef]

13. Van Vu, D.; Trinh, M.H.; Nguyen, P.D.; Ahn, H.-S. Distance-based formation control with bounded disturbances. *IEEE Control. Syst. Lett.* **2020**, *5*, 451–456. [CrossRef]

14. Pang, Z.H.; Zheng, C.B.; Sun, J.; Han, Q.L.; Liu, G.P. Distance-and velocity-based collision avoidance for time-varying formation control of second-order multi-agent systems. *IEEE Trans. Circuits Syst. II Express Briefs* **2020**, *68*, 1253–1257. [CrossRef]

15. Guo, M.; Tumova, J.; Dimarogonas, D.V. Communication-free multi-agent control under local temporal tasks and relative-distance constraints. *IEEE Trans. Autom. Control.* **2016**, *61*, 3948–3962. [CrossRef]

16. Huang, Y.; Meng, Z. Bearing-based distributed formation control of multiple vertical take-off and landing UAVs. *IEEE Trans. Control. Netw. Syst.* **2021**, *8*, 1281–1292. [CrossRef]

17. Olfati-Saber, R.; Murray, R.M. Consensus problems in networks of agents with switching topology and time-delays. *IEEE Trans. Autom. Control.* **2004**, *49*, 1520–1533. [CrossRef]

18. Oh, K.-K.; Park, M.-C.; Ahn, H.-S. A survey of multi-agent formation control. *Automatica* **2015**, *53*, 424–440. [CrossRef]

19. Montijano, E.; Cristofalo, E.; Zhou, D.; Schwager, M.; Sagues, C. Vision-based distributed formation control without an external positioning system. *IEEE Trans. Robot.* **2016**, *32*, 339–351. [CrossRef]

20. Zhao, S.; Zelazo, D. Bearing rigidity theory and its applications for control and estimation of network systems: Life beyond distance rigidity. *IEEE Control. Syst. Mag.* **2019**, *39*, 66–83. [CrossRef]

21. Gurbuz, A.C.; Cevher, V.; Mcclellan, J.H. Bearing estimation via spatial sparsity using compressive sensing. *IEEE Trans. Aerosp. Electron. Syst.* **2012**, *48*, 1358–1369. [CrossRef]

22. Flores-Resendiz, J.F.; Aranda-Bricaire, E. A general solution to the formation control problem without collisions for first-order multi-agent systems. *Robotica* **2020**, *38*, 1123–1137. [CrossRef]

23. Dong, X.; Zhou, Y.; Ren, Z.; Zhong, Y. Time-varying formation tracking for second-order multi-agent systems subjected to switching topologies with application to quadrotor formation flying. *IEEE Trans. Ind. Electron.* **2016**, *64*, 5014–5024. [CrossRef]

24. Wu, X.; Wu, Y.; Xu, Z.; Chen, Q. Fixed-time flocking formation of nonlinear multi-agent system with uncertain state perturbation. *Int. J. Control.* **2023**, *96*, 2146–2156. [CrossRef]

25. Trinh, M.H.; Mukherjee, D.; Zelazo, D.; Ahn, H. Formations on directed cycles with bearing-only measurements. *Int. J. Robust Nonlinear Control.* **2018**, *28*, 1074–1096. [CrossRef]

26. Tang, Z.; Cunha, R.; Hamel, T.; Silvestre, C. Relaxed bearing rigidity and bearing formation control under persistence of excitation. *Automatica* **2022**, *141*, 110289. [CrossRef]

27. Zhao, S.; Li, Z.; Ding, Z. Bearing-only formation tracking control of multiagent systems. *IEEE Trans. Autom. Control.* **2019**, *64*, 4541–4554. [CrossRef]

28. Wu, K.; Hu, J.; Lennox, B.; Arvin, F. Finite-time bearing-only formation tracking of heterogeneous mobile robots with collision avoidance. *IEEE Trans. Circuits Syst. II Express Briefs* **2021**, *68*, 3316–3320. [CrossRef]

29. Garanayak, C.; Mukherjee, D. Bearing-only formation control with bounded disturbances in agents' local coordinate frames. *IEEE Control. Syst. Lett.* **2023**, *7*, 2940–2945. [CrossRef]

30. Luo, X.; Li, X.; Li, X.; Guan, X. Bearing-only formation control of multi-agent systems in local reference frames. *Int. J. Control.* **2021**, *94*, 1261–1272. [CrossRef]

31. Zhang, Y.; Xingjian, W.; Shaoping, W.; Xinyu, T. Distributed bearing-based formation control of unmanned aerial vehicle swarm via global orientation estimation. *Chin. J. Aeronaut.* **2022**, *35*, 44–58. [CrossRef]

32. Yang, Z.; Chen, C.; Zhu, S.; Guan, X.-P.; Feng, G. Distributed entrapping control of multiagent systems using bearing measurements. *IEEE Trans. Autom. Control.* **2020**, *66*, 5696–5710. [CrossRef]

33. Wu, X.; Dong, Y. An internal-model-based event-triggered strategy for rendezvous with connectivity preservation problem of multi-agent systems. *Int. J. Robust Nonlinear Control.* **2022**, *32*, 8874–8888. [CrossRef]

34. Dong, X.; Yu, B.; Shi, Z.; Zhong, Y. Time-varying formation control for unmanned aerial vehicles: Theories and applications. *IEEE Trans. Control. Syst. Technol.* **2014**, *23*, 340–348. [CrossRef]

35. Zhao, S.; Zelazo, D. Localizability and distributed protocols for bearing-based network localization in arbitrary dimensions. *Automatica* **2016**, *69*, 334–341. [CrossRef]

36. Liu, Q.; Ye, M.; Qin, J.; Yu, C. Event-triggered algorithms for leader–follower consensus of networked Euler–Lagrange agents. *IEEE Trans. Syst. Man Cybern. Syst.* **2017**, *49*, 1435–1447. [CrossRef]

37. Zhang, Y.; Wang, S.; Wang, X.; Tian, X. Bearing-based formation control for multiple underactuated autonomous surface vehicles with flexible size scaling. *Ocean Eng.* **2023**, *267*, 113242. [CrossRef]

38. Zhang, Y.; Li, S.; Wang, S.; Wang, X.; Duan, H. Distributed bearing-based formation maneuver control of fixed-wing UAVs by finite-time orientation estimation. *Aerosp. Sci. Technol.* **2023**, *136*, 108241. [CrossRef]

39. Van Tran, Q.; Kim, J. Bearing-constrained formation tracking control of nonholonomic agents without inter-agent communication. *IEEE Control. Syst. Lett.* **2022**, *6*, 2401–2406. [CrossRef]

40. Li, X.; Wen, C.; Chen, C. Adaptive formation control of networked robotic systems with bearing-only measurements. *IEEE Trans. Cybern.* **2020**, *51*, 199–209. [CrossRef]

41. Su, H.; Chen, C.; Yang, Z.; Zhu, S.; Guan, X. Bearing-based formation tracking control with time-varying velocity estimation. *IEEE Trans. Cybern.* **2022**, *53*, 3961–3973. [CrossRef] [PubMed]

42. Drazin, P.G. *Nonlinear Systems*; Cambridge University Press: Cambridge, UK, 1992.